Journal of Coastal Conservation (2024) 28:66
https://doi.org/10.1007/s11852-024-01065-y

Towards sustainable coastal management: a hybrid model for vulnerability and risk assessment

Ahmet Durap[1,2,4] · Can Elmar Balas[3]

Received: 20 May 2024 / Revised: 2 July 2024 / Accepted: 9 July 2024

Abstract

This paper presents the development of a Hybrid Model (HM) integrated with a Bayesian Network (BN) for comprehensive coastal vulnerability and risk assessment, with a focus on Konyaaltı Beach, Antalya, Turkey. The HM incorporates critical environmental parameters such as wind, waves, currents, and sediment transport to simulate conditions at vulnerable coastal areas and perform risk assessments for storm effects, flooding, and erosion. The model includes submodules for predicting coastal storms, quantifying sediment transport rates, assessing tsunami inundation severity, and categorizing storms based on beach typologies. The Adaptive Neuro-Fuzzy Inference System (ANFIS) is utilized for significant wave height predictions, enhancing the model's accuracy. The integration of hydrodynamic modeling, Bayesian networks, and ANFIS offers a robust framework for assessing coastal vulnerability and informing sustainable management practices. The study's results highlight the necessity for integrated risk management strategies, including adaptive infrastructure design, zoning and land use regulations, ecosystem-based management, and continuous monitoring and model refinement to enhance coastal resilience against dynamic environmental forces. This research provides valuable insights for mitigating the impacts of hazards on urban developments, contributing to the advancement of sustainable coastal management.

Keywords Coastal vulnerability · Vulnerability trends · Bayesian Networks · ANFIS · Storm and Beach classifications

Introduction

The world's coastlines, stretching for hundreds of thousands of kilometers, are vibrant ribbons of life (Sheaves et al. 2015). They teem with diverse ecosystems, provide vital resources for human populations, and serve as critical economic engines through tourism, fisheries, and maritime trade (BRIONES-PEÑALVER et al. 2023; Kosenius and Markku 2015). However, these very same coastlines are on the front lines of a changing planet. Rising sea levels, intensifying storms, and coastal erosion, all exacerbated by climate change, threaten to reshape these landscapes and disrupt the delicate balance they support (Hanak and Moreno 2012; Paprotny et al. 2021; Toimil et al. 2017; Zhang et al. 2004). To navigate this uncertain future, coastal communities, like those bordering the iconic Konyaaltı Beach in Turkey, require a robust understanding of their vulnerability and risk.

Coastal vulnerability refers to the susceptibility of a coastal system to the adverse impacts of hazards (Sheik Mujabar and Chandrasekar 2013). These hazards can be natural, such as storm surges, tsunamis, and long-term sea level rise, or human-induced, such as pollution and unsustainable development practices. The vulnerability of a particular location is not simply a function of the hazard itself, but rather a complex interplay of physical, ecological, social, and economic factors (Mohanty et al. 2020). Physical factors like geomorphology, sediment composition, and bathymetry can influence a coastline's ability to withstand erosion or inundation (Mani Murali et al. 2013). Ecological factors, such as the presence of wetlands or mangroves, can provide natural buffers against storm surge and play a crucial role in maintaining coastal health (Chen et al. 2023).

✉ Ahmet Durap
ahmetdurap@gmail.com

1 Division of Civil Engineering, The University of Queensland, Brisbane 4072, Australia

2 Division of Coastal Sciences and Engineering, Civil Engineering Department, Civil Engineering Faculty, Istanbul Technical University, Maslak 34469, Istanbul, Turkey

3 Faculty of Engineering, Civil Engineering Department, Gazi University, Celal Bayar Bulvarı, 06570 Ankara, Maltepe, Turkey

4 Engineering and Natural Sciences Faculty, Istanbul Medipol University, 34181, Beykoz, İstanbul, Türkiye

Social and economic factors, including population density, infrastructure development, and economic dependence on coastal resources, further contribute to a region's vulnerability (Lapietra et al. 2023).

Coastal vulnerability assessments (CVAs) aim to identify and quantify these various factors, ultimately creating a map of vulnerability along a coastline (Filippaki et al. 2023). This map provides a powerful tool for coastal managers, allowing them to prioritize areas of highest concern, like Konyaaltı Beach, and allocate resources effectively. CVAs employ a variety of methodologies, ranging from simple scoring systems based on readily available data to complex computer models incorporating sophisticated physical processes (Torresan et al. 2008).

However, vulnerability alone does not tell the whole story. Coastal risk assessments (CRAs) take the next step by estimating the potential consequences of these hazards on exposed communities and infrastructure (Durap and Balas 2022; Tahri et al. 2017). By combining information on vulnerability with data on hazard probability and intensity, CRAs can paint a clear picture of the potential economic, social, and environmental impacts of coastal hazards on locations like Konyaaltı Beach.

The integration of vulnerability and risk assessments is essential for developing effective coastal management strategies (Mafi-Gholami et al. 2019). By understanding both the susceptibility of a region and the potential consequences of hazards, coastal managers can prioritize areas for adaptation and mitigation efforts. Adaptation strategies aim to adjust human systems to accommodate the changing environment, such as building seawalls or elevating infrastructure (Mendoza and Jiménez 2009; Sudha Rani et al. 2015). Mitigation strategies, on the other hand, focus on reducing the severity of the hazards themselves, often through emission reduction measures to combat climate change (Lin et al. 2012).

Türkiye, a nation bordered by the Mediterranean, Aegean, Marmara, and Black Seas, boasts an extensive coastline of approximately 8,500 km (excluding islands). This coastline exhibits remarkable heterogeneity, with distinct regional variations. These variations can be attributed to a multitude of factors influencing water density, including salinity, coastal slope, precipitation patterns, soil composition, seagrass meadows, beach width, and vegetation growth rates. Consequently, a region-specific (e.g.,(Arda et al. 2024; Aykut and Tezcan 2024; Özyurt and Ergin 2010)) approach is necessary to effectively manage and conserve this diverse coastal environment.

For instance, Aykut and Tezcan (2024) investigated sea level rise in specific areas of the Mediterranean Sea, while Arda et al. (2024) examined the Marmara Golf Region. Özyurt and Ergin (2010) focused on the Göksu Delta, but none of these studies incorporated sensitivity analyses to identify the most influential parameters in coastal vulnerability calculations.

This paper delves deeper into the key components of coastal vulnerability and risk assessments, aiming to enhance sustainable coastal management in a changing environment including sensitivity assessment. Our focus is on the various methodologies employed, their strengths and limitations, and the importance of these assessments for protecting treasured destinations like Konyaaltı Beach. The primary purpose of this research is to address the critical need for a holistic approach to coastal vulnerability and risk assessment, particularly through the integration of environmental parameters such as wind, waves, currents, and sediment transport.

We aim to answer the following research questions: How can integrated models improve the prediction and mitigation of coastal hazards? What is the effectiveness of ANFIS models in predicting significant wave heights for coastal and marine structure design? How can a Hybrid Model alongside Bayesian Network (BN) Model be developed to assess coastal vulnerability?

Our main findings indicate that the alignment of model predictions with real-world data underscores the critical role of long-term wave prediction studies for the resilience of coastal and marine structures against dynamic natural forces. The study highlights the effectiveness of combining hydrodynamic modeling, Bayesian networks, and ANFIS to simulate conditions at vulnerable beaches and perform risk assessments for various hazard indexes, including storm effects, flooding, and erosion. A novel emphasis on tsunami inundation and river flooding as key components of the Coastal Vulnerability Index (CVI) marks a significant advancement in coastal vulnerability studies.

The paper is structured as follows: Section "Methodology" reviews some relevant literature and identifies gaps in current research. Section "Case study in Konyaalti, Turkey" details the study area, including the development and application of the Hybrid Model and Bayesian Network Model. Section "Results" presents the results and discusses their implications for coastal management. Finally, Section "Discussions" concludes with a summary of findings and recommendations for future research and coastal management practices.

Methodology

This section details the methodology behind a Hybrid Model (HM) that combines a 3D Hydrodynamic Transport Model and a Bayesian Network (BN) for assessing coastal vulnerability at Konyaaltı Beach, Turkey. This unique combination unlocks a holistic understanding of coastal risks, enabling us to effectively evaluate the interplay between various environmental forces.

The HM acts as a framework, considering critical parameters such as wind, waves, currents, and sediment transport. These parameters play a fundamental role in shaping coastal landscapes and influence phenomena like storms, flooding, and erosion. By incorporating these variables, the HM equips us to not only assess the current state of the coast but also forecast potential future vulnerabilities.

The core of this methodology is the coastal vulnerability alongside risk, which integrates several submodules.These submodules act as individual experts, each focusing on a specific coastal threat:

- Coastal storms prediction: This submodule meticulously analyzes atmospheric and oceanic data to predict the likelihood and intensity of future storms.
- Sediment transport rate quantification: This submodule delves into the dynamics of sediment movement along the coast, providing crucial insights into erosion and accretion patterns.
- Tsunami inundation severity assessment: This submodule evaluates the potential impact of tsunamis, considering factors like wave height and run-up distance.
- Storm categorization based on beach types: By classifying beaches as reflective or dissipative, this submodule refines our understanding of how different coastal morphologies respond to storm events.

The case study of Konyaaltı Beach serves as a compelling illustration of the HM's capabilities. By calculating the CVI for this specific location, researchers can gain valuable insights into the beach's vulnerability to various coastal hazards. This knowledge empowers us to develop more effective coastal management strategies, ensuring the long-term sustainability of our shorelines.

ANFIS storm prediction module

The prediction of the design of significant wave heights (H_s) has become a challenging issue in light of the notable impacts of climate change in recent years. This study aimed to obtain wave predictions using Adaptive Neuro-Fuzzy Inference System (ANFIS) in a time series analysis framework. The Sugeno Fuzzy Models (SFM) were developed using a fuzzy inference mechanism, incorporating various layers and nodes defined by unique membership functions.

The 24-h daily data for the dataset from the buoy station measurements in the Gulf of Antalya from March 2015 to January 2017 was obtained (Fig. 1). The acquired buoy data had gaps of 1–2 h. These missing data were filled in using developed ANFIS models. Therefore, ANFIS model was used to estimate the missing wave data in the model. Depending on the model, the missing data gaps were addressed, and the dataset was enhanced. The neuro-fuzzy design application of MATLAB R2013a was used to develop the model. Out of 8,779 significant wave height (Hs) data points for 2015–2016, 6,618 were used for the learning phase of the model, and 2,161 were used for the testing phase. For the train and test datasets, ANFIS models were created by combining data columns with time lags of t-5, t-4, t-3, t-2, and t-1 to predict the t time. Separate prediction results were obtained for both training and testing. The t-5, t-4, t-3, t-2, and t-1 time data steps in the train and test datasets are input parameters, while the values in the t column are the measurement values against which the output parameters will be compared. For example, the Hs-3–1 model includes t-3 and t-1 time steps in the train and test datasets as input parameters to predict the missing data at the t time step, as defined in Table 7.

ANFIS combines the fast and simple training algorithms of ANN with the expert knowledge of FL, resulting in more precise and coherent predictions compared to the individual use of these techniques. The ANFIS models developed in this study utilized a fuzzy inference mechanism with two

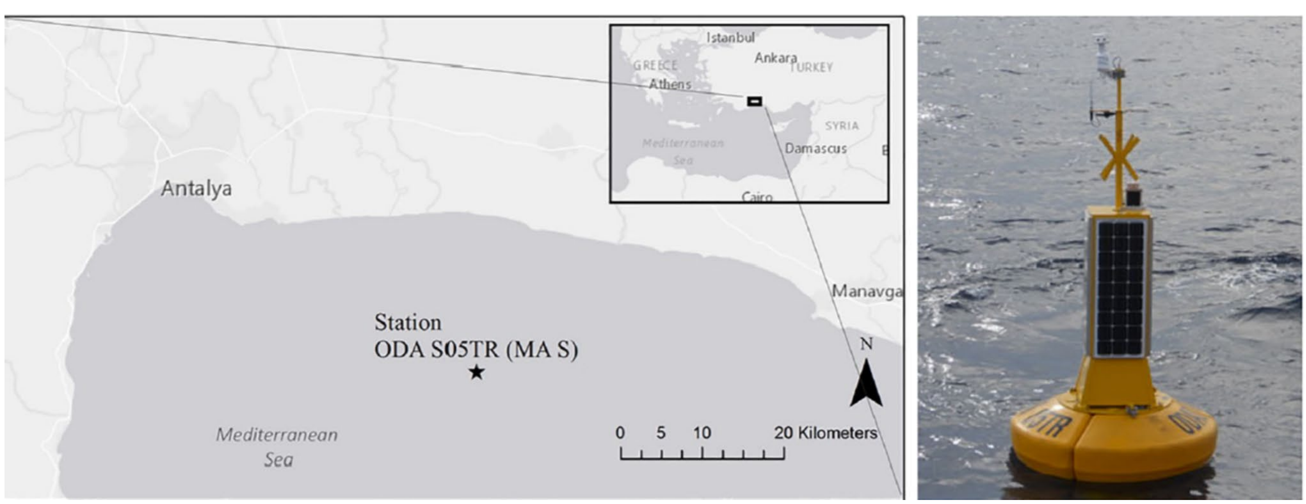

Fig. 1 The buoy station (star) is located on the Antalya coast

inputs (x, y) and an output (z). Sugeno Fuzzy Models were constructed, consisting of various layers and nodes, defined by unique membership functions. The ANFIS structure was created by using five distinct layers as given in Fig. 1:

i. In Layer 1, the membership degree of the fuzzy set is determined with the help of the membership functions at each node as indicated in Eq. 1.

$$\begin{aligned} R_{1,i} &= \mu_{Ai}(x),\ i = 1,2 \\ R_{1,i} &= \mu_{Bi-2}(y),\ i = 1,2 \\ R_{1,i} &= \mu_{Ai}(x),\ i = 1,2 \\ R_{1,i} &= \mu_{Bi-2}(y),\ i = 1,2 \end{aligned} \tag{1}$$

where x and y are the certain (crisp value) input values at node i, A_i and B_i are the fuzzy linguistic terms, and μ_{Ai} and μ_{Bi} represent the fuzzy membership functions.

Several membership functions were utilized, including Gauss, Gumbel, triangle, trapezoid, sigmoidal, etc. The results of the statistical performance parameters showed that the Gauss and Gumbel membership functions provided the most accurate wave predictions. Hence, the Gauss and Gumbel-type membership functions were used in the study and their results were compared with those obtained from time series models. The Gauss membership function is depicted by Eq. 2 in the form of a bell curve.

$$\mu_{A_i} = \frac{1}{1 + \left[\left(\frac{x-c_i}{a_i}\right)^2\right]^{b_i}} \tag{2}$$

where, $\{a_i, b_i, c_i\}$ are the variables controlling the skewness of the membership functions of IF–THEN fuzzy rule structures (Fig. 2).

ii. Layer 2 is the layer in which the degrees of the first-order two rules are calculated in form of a product by using the "and" logical operator as expressed in Eq. 3.

$$\begin{aligned} &R_{2,k} = w_k = \mu_{Ai}(x)x\ \mu_{Bj}(y), \\ &k = 1, \ldots, 4\ i = 1,2;\ j = 1,2 \end{aligned} \tag{3}$$

iii. Layer 3 is the layer where the ratio of the degree of the i^{th} rule at the i^{th} node to the sum of the accomplishment levels of all rules is calculated as presented in Eq. 4.

$$R_{3,i} = \overline{w_i} = \frac{w_i}{\sum_{k=1}^{4} w_k} i = 1, \ldots, 4 \tag{4}$$

iv. Layer 4 is the layer in which the contribution of each i^{th} rule among the total output is calculated as provided in Eq. 5.

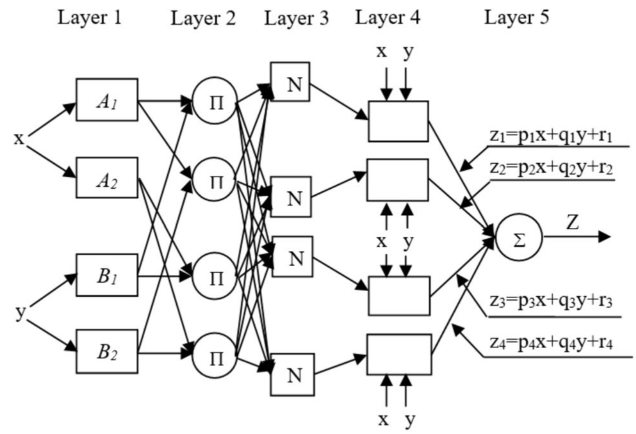

Fig. 2 The ANFIS structure of SFM with two inputs and four rules

$$R_{4,i} = \overline{w_i} f_i = \overline{w_i}(p_i x + q_i y + r_i), i = 1, \ldots, 4 \tag{5}$$

where, $\overline{w_i}$ is the output value of the i^{th} node in the preceding layer.

v. Layer 5 is the layer at which the total output is calculated by using all the incoming signals. At this layer, only one quantity is obtained by de-fuzzifying the rules.

$$R_{5,i} = \sum_{i=1}^{4} \overline{w_i} f_i = \frac{\sum_{i=1}^{4} w_i f_i}{\sum_{i=1}^{4} w_i} \tag{6}$$

Various statistical performance indicators were calculated to evaluate the successes of the models developed within the scope of this study. The equations of these statistical parameters, such as Root Mean Square Error (RMSE), Mean Absolute Error (MAE), Correlation Coefficient (R), Determination Coefficient (R^2), and Nash–Sutcliffe Efficiency (NSE) [30] are presented by Eqs. (7), (8), (9), (10) and (11), respectively.

$$RMSE = \sqrt{\frac{\sum_{t=1}^{n} \left(y_t^o - y_t^p\right)^2}{n}} \times 100 \tag{7}$$

$$MAE = \frac{1}{n} \sum_{t=1}^{n} \left| y_t^o - y_t^p \right| \tag{8}$$

$$R = \frac{\sum_{t=1}^{n} (y_t^o - \overline{y^o})(y_t^p - \overline{y^p})}{\sqrt{\sum_{t=1}^{n} (y_t^o - \overline{y^o})^2 \sum_{t=1}^{n} (y_t^p - \overline{y^p})^2}} \tag{9}$$

$$R^2 = \left(\frac{\sum_{t=1}^{n} (y_t^o - \overline{y^o})(y_t^p - \overline{y^p})}{\sqrt{\sum_{t=1}^{n} (y_t^o - \overline{y^o})^2 \sum_{t=1}^{n} (y_t^p - \overline{y^p})^2}} \right)^2 R^2 = \left(\frac{\sum_{t=1}^{n} \left(y_t^o - \overline{y^o}\right)\left(y_t^p - \overline{y^p}\right)}{\sqrt{\sum_{t=1}^{n} \left(y_t^o - \overline{y^o}\right)} \sqrt{\sum_{t=1}^{n} \left(y_t^p - \overline{y^p}\right)}} \right)^2 \tag{10}$$

$$NSE = 1 - \frac{\sum_{t=1}^{n} \left(y_t^o - y_t^p\right)^2}{\sum_{t=1}^{n} \left(y_t^o - \overline{y^o}\right)^2} \tag{11}$$

where y_t^o is the observed value, y_t^p is the estimated value and n is the number of observations.

Hydrodynamic coastal morphology module

Hydrotam-3D is a three-dimensional hydrodynamic, sediment transport, and water quality model validated by utilising several experimental and analytical data published in the literature since 1990; its effective usage for a range of real-world applications along the Turkish coastline has been proved (Balas 2004; Balas and Özhan 2001, 2002, 2003).

The Hydrodynamic Sediment Transport Model is supported by the geographic information system (GIS) and cloud computing. The model database includes bathymetries of all Turkish coasts, hourly wind data since the establishment of Turkish Coastal Meteorological Stations (MS), and all measured physicochemical data at the sites.

Tsunami inundation module

Two Multi-Layer Perceptrons (MLP) neural networks) were formed to predict the intensity of an earthquake that has the potential to trigger a tsunami. in the years to come and to make an estimate regarding the probable height of a tsunami inundation that may strike the coast of the Aegean Seas (Balas and Ergin 2003). It encompasses two artificial neural networks (ANN) to predict the earthquake magnitude that could potentially generate a tsunami in future to estimate the probable tsunami inundation height that may transpire along the coast. Network-1 is constructed to input the earthquake depth and the return period to forecast the magnitude Mw. The general structure of ANN is given in Fig. 1. The structure of Network-1 is designed in the form $X_2Y_{50}Z_1$, indicating two nodes in the input layer, one node in the output layer, and the hidden layer containing 50 nodes. For Network-2, tsunami intensity, earthquake magnitude, and depth are input values to predict the tsunami risk along the coast. The structure of Network-2 is established in the form $X_3Y_{10}Z_1$, indicating three nodes in the input layer, one node in the output layer, and the hidden layer containing 10 nodes.

The first artificial neural network, "Network-1, "is obtained for the earthquake magnitude estimation, which may create a tsunami in the following years. The data is divided into three occurrence regions: Marmara, Aegean, and Mediterranean. The return period of two successive tsunamis is calculated for each region to be used as an input in the network. The inputs and outputs of Network-1 are given in Table 1. The data range used in the Network-1 is tabulated in Table 2 (Fig. 3).

The total number of data used in Network-1 is 113, of which about 60% is used in the training phase. The obtained network parameters are given in Table 3.

where;

It	Iteration number
R	Correlation Value
x	number of node in the input layer
y	number of node in the hidden layer
z	number of node in the output layer
γ	adaptive learning rate
α	momentum rate
MSE	mean square error

A trial and error process determines the number of iterations to obtain the best correlation value and acceptable mean square error. The second artificial neural network, "Network-2, "is obtained for the tsunami height estimation. The data used for "the Network-2" from Table 4 as input and outputs is given in Table 5, and the data range is illustrated in Table 6.

The total data used in Network-2 is 30, of which about 61% is used in the training phase. The obtained network parameters are given in Table 7.

Where;

It	Iteration number
R	Correlation Value
x	number of node in the input layer
y	number of node in the hidden layer
z	number of node in the output layer
γ	adaptive learning rate
α	momentum rate
MSE	mean square error

Region codes were defined to differentiate the Marmara, Aegean, and Mediterranean Seas. These codes, along with

Table 1 ANFIS model types and membership functions used

ANFIS Model	Structure	Learning Iteration	Optimization model	Membership function
Hs 3 1	Hs(t) = Hs(t-3), Hs(t-1)	200	hybrid-constant	gbellmf
Hs 3 1	Hs(t) = Hs(t-3), Hs(t-1)	200	hybrid-constant	gaussmf
Hs 3 1	Hs(t) = Hs(t-3), Hs(t-1)	300	hybrid-constant	trapmf
Hs 3 1	Hs(t) = Hs(t-3), Hs(t-1)	200	hybrid-constant	trimf
Hs 3 1	Hs(t) = Hs(t-3), Hs(t-1)	200	hybrid-constant	gauss2mf
Hs 5 3 1	Hs(t) = Hs(t-5), Hs(t-3), Hs(t-1)	200	hybrid-constant	gbellmf
Hs 5 3 1	Hs(t) = Hs(t-5), Hs(t-3), Hs(t-1)	200	hybrid-constant	gaussmf
Hs 5 3 1	Hs(t) = Hs(t-5), Hs(t-3), Hs(t-1)	120	hybrid-constant	gauss2mf
Hs 4 3 1	Hs(t) = Hs(t-4), Hs(t-3), Hs(t-1)	120	hybrid-constant	gbellmf
Hs 4 3 1	Hs(t) = Hs(t-4), Hs(t-3), Hs(t-1)	120	hybrid-constant	gaussmf
Hs 4 3 1	Hs(t) = Hs(t-4), Hs(t-3), Hs(t-1)	200	hybrid-constant	gauss2mf
Hs 4 3 1	Hs(t) = Hs(t-4), Hs(t-3), Hs(t-1)	300	hybrid-constant	gbellmf

Table 2 Inputs and Outputs of Network-1

INPUTS			OUTPUT
Region Code	Earthquake Depth (d)	Return Period (R_p)	Earthquake Magnitude (M_s)
1 (Marmara)			
2 (Aegean)			
3 (Mediterranean)			

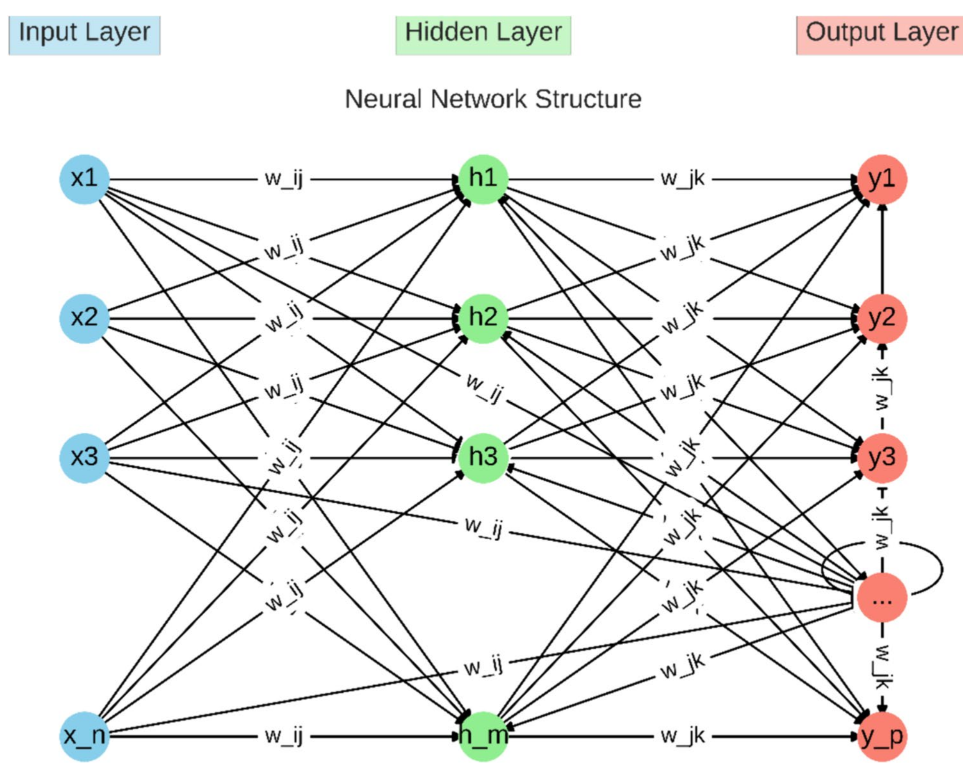

Fig. 3 Structure of ANN

earthquake depth and return period, were used as inputs for Network-1 to predict the earthquake magnitude Ms. The structure of Network-1 was designed as x3y50z1, indicating three nodes in the input layer, 50 nodes in the hidden layer, and one node in the output layer. The gradient descent algorithm was employed with an optimal momentum rate of 0.5

Table 3 The Data Range Used in the Network-1

Variable	d	R_p	M_s
Maximum	80	970	7.6
Minimum	10	1	4.9

Table 4 Network-1 parameters

It	70.000
R	0,965
x–y-z	3–50-1
γ	0,001
α	0,5
MSE	0,00985293

Table 6 Data Range Used in the Network-2

Variable	M_s	d	i
Maximum	7.9	80	6
Minimum	4.8	4.0	0

Table 7 Network-2 parameters

It	5.000
R	0,972
x–y-z	3–10-1
γ	0,001
α	0,5
MSE	0,000034

and an adaptive learning rate of 0.001. A sigmoid bipolar function was used in the hidden layers, while a linear function was applied in the output layer. The network was developed iteratively using trial and error. After 60,000 iterations, a satisfactory correlation value of R = 0.965 was achieved, with a mean square error (MSE) of 0.00985293.

For Network-2, the input values included tsunami intensity, earthquake magnitude, and depth to predict tsunami wave height along the Marmara and Aegean Seas coasts. Similar to Network-1, this network was developed using trial and error to determine the optimal adaptive learning rate, considering the database. The structure of Network-2 was designed as x3y10z1, indicating three nodes in the input layer, 10 nodes in the hidden layer, and one node in the output layer. The momentum and adaptive learning rates were set at 0.5 and 0.001, respectively. After 5,000 iterations, a satisfactory correlation value of R = 0.972 was obtained, with an MSE of 0.000034 during the testing stage. The gradient descent algorithm was used with a bipolar sigmoid function in the hidden layers and a linear activation function in the output layer.

BN-coastal vulnerability module

A system for categorizing storms based on the amount of energy they carried was developed in this paper and tabulated in Table 1, where; Hs is the significant wave height (m); Tp is the storm peak period (sec), and N is the number of storms observed during 10 years. Table 8 is the key in which the wave energy range is used to designate whether a storm is mild or severe. Hence, the wave energy range [E] is a useful reference for classifying various types of storms.

The novel approach of the Coastal Vulnerability Assessment Model (CVAM) is illustrated in Fig. 4, in which the methodology is divided into five separate phases. Categorization for dissipative and reflective beaches was constructed using 5 categories, class 1 through class 5. These classes were ordered from least reflective to most reflective and the results are shown in Tables 9 and 10.

This paper is aiming for reflective beaches to delineate coastal morphology in terms of shoreline patterns. Shoreline change or patterns offers invaluable insight into a coastal vulnerability or erosion-prone hotspots. Consequently, 498 storms have been recorded throughout the last decade, and their energy levels (from weak to severe), run-up values (for dissipative and reflective), severity, duration, periods, and significant wave heights have all been recorded and tabulated in Tables 7 and 9.

Uncertainties connected to the prediction models that were employed, the climatic conditions, and the morphology of the coastline will impact the hazard evaluation of the shoreline (Durap et al. 2023). Bayesian Networks (BN) are employed as an efficient approach for addressing the problem since it facilitates the incorporation of these uncertainties, simultaneously defining the system behavior stochastically and providing insight into the relationships among relevant variables Fig. 4. Bayesian Networks (BN) can characterize the system response more accurately. A BN-based technique for assessing the risk of storm-induced damage at a regional scale is developed in this paper.

The storm intensity scale was created using data from a directional wave time series obtained from the wave buoy with additional data predicted by the ANFIS Method and found that there were 498 storms detected in the data set.

Table 5 Inputs and Outputs of the Network-2

INPUTS			OUTPUT
Earthquake Magnitude (M_s)	Earthquake Depth (d)	Tsunami Intensity (i)	Average Tsunami Wave Height at the Coast (H_{av})

Table 8 Storm types based on wave energy (E: m^2sec) content

Strom parameters and energy content (E) range		Storm class				
		Weak (1)	Moderate (2)	Significant (3)	Severe (4)	Extreme (5)
Mean Values	N	246	137	100	14	1
	t (hours)	12	52	85	86	161
	Hs (m)	2	3.5	4	5.1	6.1
	Tp (s)	6.2	11	8.5	12	8
	E (m^2 sec)	32	350	550	950	1460

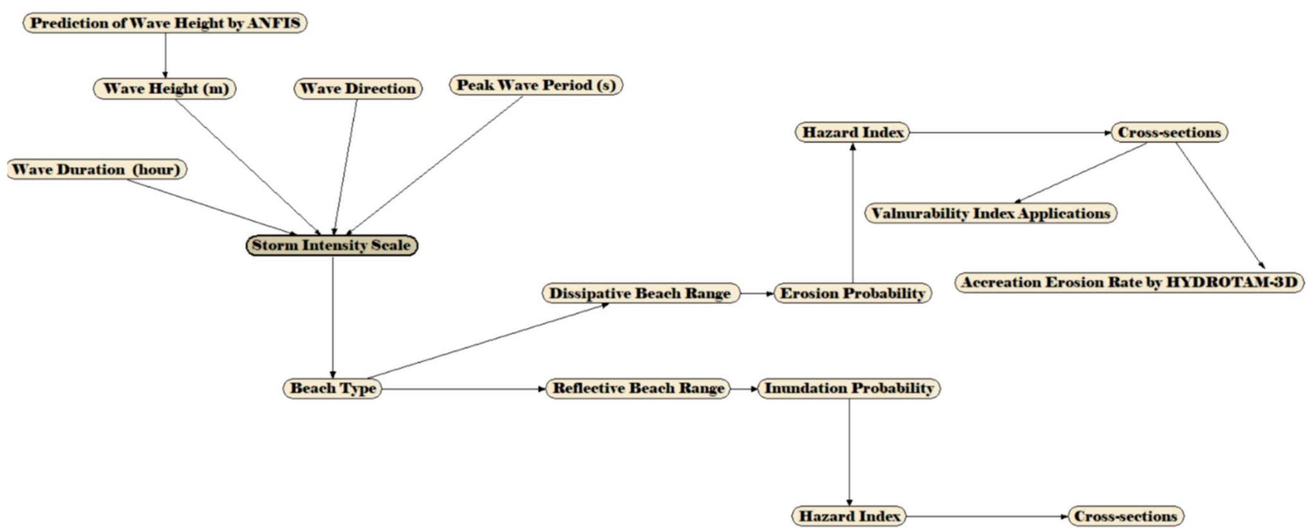

Fig. 4 The novel approach of Coastal Vulnerability Assessment Model (CVAM): Methodology of evaluating vulnerable coasts to storms

Table 9 Wave energy content and storm classifications

Energy range	24 ≤ Energy ≤ 250	Weak
	250 ≤ Energy ≤ 500	Moderate
	501 ≤ Energy ≤ 700	Significant
	701 ≤ Energy ≤ 1200	Severe
	Energy ≥ 706.9	Extreme

Table 10 Beach classifications run-up table

	Reflective range (Eq. 15)		Dissipative range (Eq. 14)	
Classification	Range	N	Run up ≤ 1.2	N
1	Run up ≤ 1.6	284	1.2 ≤ Run up ≤ 1.6	196
2	1.6 ≤ Run up ≤ 2.1	76	1.6 ≤ Run up ≤ 2.2	188
3	1.6 ≤ Run up ≤ 2.1	64	2.2 ≤ run up ≤ 2.8	66
4	1.6 ≤ run up ≤ 2.1	47	Run up > 2.8	42
5	Run up > 3.3	21	Run up ≤ 1.2	8

Authors of this paper have utilized the energy content (E), which is specified in Eq. (12), to describe the storm's intensity:

$$E = \int_{t2}^{t1} Hs^2 dt \tag{12}$$

The time range in which Hs (t) > 1.5 m occurs is defined by the values of t1 and 12. Other definitions of the energy content used in literature, such as relative storm power, constitute a relatively simple approach to calculating storm energy but can underestimate or overestimate the real energy contained in a storm.

This study decreased the initial selection of 498 storms to 30 clusters. This technique produced a 5-storm classification that is comparable to the commonly used Tropical Cyclones Scale and the Atlantic coast North-east Storms Strength Scale. According to this classification, the Turkish Mediterranean coast wave storm strength scale is considered weak, moderate, major severe, and extreme storms. Beach characteristics in the region are defined by considering two parameters:

Dean parameter D

This dimensionless parameter was first established by Gourlay, and Dean recommended using it as a beach profile change predictor (1973). It assumes that most of the sediment movement that occurs offshore takes place in suspension.

It is based on the theory that the waves put the sediment into suspension, and after reaching its maximum height above the bottom, the cumulative transport is determined by a relation between the amount of time it takes the particle to fall and the semi-period of waves that are incident on it, as given by Eq. (13).

$$\mathrm{D} = \frac{H_b}{(WsT)} \tag{13}$$

where H_b is breaker height, Ws is the fall velocity of the sediment and T is the zero up crossing wave period.

Run-up scale

A beach slope value of 0.07 was used in the estimation of run-up for dissipative beaches using the method of Mase. The Rs, or substantial run-up, is determined by Eq. (14):

$$R_s^T = 0.725 g^{0.35} \tan\beta^{0.70} H_0^{0.65} T^{0.7} \tag{14}$$

For the reflective beach type, researchers of this paper determined the run-up value by using the method developed by Holman and Sallenger, which resulted in a value of 0.12 for tan ß as indicated in Eq. (15).

$$R_s^T = 0.307 g^{0.5} \tan\beta H_0^{0.5} T \tag{15}$$

where R stands for significant run-up, g is the acceleration of gravity, tanβ is the beach slope, H_0 is the significant wave height in deep water, and T is the wave period.

Coastal vulnerability index (CVI)

One of the earliest methods for determining potential vulnerability was modified from Gornitz's (1990, 1991) work, which focused on seven variables that had a significant impact on coastal transformation while using the U.S. shoreline on a nationwide scale. The general CVI is determined by dividing the entire number of variables by the square root of the variable product (n) as given in Eq. (16).

$$CVI = \sqrt{\frac{a_1 * a_2 * a_3 * a_4 * a_5 * a_6}{6}} \tag{16}$$

a1 geomorphology/landform
a2 shoreline slope
a3 relative sea-level change
a4 shoreline change rates
a5 significant wave height
a6 tidal range

Equation (16) is used to generate the cumulative CVI score for all of the various coastal sections that come together to create the domestic shoreline. This value is derived by plugging the vulnerability class values into the equation. After that, the vulnerability groups are expressed by percentages ranging from 0–25%, 25–50%, 50–75%, and to 75–100%. These ranges are based on the percentiles of the whole group. To put it another way, a vulnerability score of 1 indicates the least amount of risk, while a vulnerability score of 4 indicates the greatest amount of risk.

(Koroglu et al. 2019) applied six variables to assess Barcelona Province's coastal vulnerability in terms of five different coastal vulnerabilities from 1 to 5. Since the study area has a river, known as Boğaçay, the authors considered two new variables as in Tables 11 and 12.

Accordingly, CSI is taking the form Eq. (17).

$$CVI = \sqrt{\frac{a_1 * a_2 * a_3 * a_4 * a_5 * a_6 * a_7 * a_8}{8}} \tag{17}$$

Case study in Konyaalti, Turkey

The provinces of Antalya and Muğla, as well as parts of Aydın, southern İzmir, and western Mersin, constitute the region of south-west Turkey known as the Turkish Riviera, also known as the Turquoise Coast. This section of Turkey's shoreline along the Aegean and Mediterranean Seas is a popular national and international tourist destination due to its pleasant temperature, mild sea, picturesque mountains, good beaches, and plenty of natural and archaeological landmarks to see. It is generally agreed that Konyaaltı Beach in Antalya Bay, located on the Turkish Riviera to the west of Antalya, is the most popular beach in the city and is also regarded as one of the most popular venues for the Antalya area. Konyaaltı Beach has been awarded the prestigious "Blue Flag," certifying the high standard of its facilities and water. Hence, Antalya Bay was determined as the study area as the diamond part of the Turkish Riviera. Antalya Bay is located on the southern coast of Turkey, on the Mediterranean coast. The geographical location of Antalya Bay is 36° 46′ 18″ North and 30° 57′ 20″ East. The total coastal length of this gulf, which starts from the Anamur cape in the east and extends to the Kırşığı cape in the west, is 450 km (Fig. 5).

The Konyaaltı Beach in Antalya, Turkey, serves as a critical case study for assessing coastal vulnerability and implementing sustainable coastal management practices. This region, part of the broader Turkish Riviera, is renowned for its significant tourism appeal, characterized by its picturesque landscapes, historical and archaeological sites, and the Blue Flag-certified Konyaaltı Beach. However, the area faces substantial risks from coastal erosion, flooding, and

Table 11 Ranking of coastal sensitivity index variables for Turkish coasts, adapted from the coastal risk classes of (Gornitz 1991)

	Ranking of sensitivity index				
	Very low	Low	Moderate	High	Very High
Parameters	1	2	3	4	5
Landform	Plutonic rocks, high-grade metamorphic & volcanic rocks	Metamorphic rocks	Most sedimentary rocks	Poorly consolidated sediments	Unconsolidated sediments, ice
Sea-level change (mm/yr)	Fiord, high rock cliffs, fiard	Moderate and low rock cliffs	Beach	Barrier, bluffs, salt marsh, peat, mud flat, delta, spit, tombolo	Ice-bonded sediment, ice-rich sediment, ice shelf, tidewater glacier
Shoreline displacement (m/yr)	3–50	-50 to -20	unconsolidated sediment over bedrock	21 to 40	> 40
Tidal range (m)	> +0.1	0 stable	-19 to + 20	-0.6 to -1.0 eroding	> -1.0
One-year maximum wave height (m)	accreting	0.5–1.9	-0.1 to -0.5 eroding	4.1–6.0	eroding
Coastal Slope (%)	> 12	8–12	4–8	2–4	< 2

Table 12 Taking into consideration two newly introduced CVI components for the Konyaalt Beach

New Variable	Unit	Very Low	Low	Moderate	High	Very High
		1	2	3	4	5
River Flooding ΔQ	ΔQ (m^3/s) Return Period of flood Tr (years)	Tr < 10 years ΔQ < 5 m^3/s	Tr < 100 years ΔQ < 10 m^3/s	Tr < 150 years ΔQ < 20 m^3/s	150 < Tr < 200 years 20 < ΔQ < 50 m^3/s	Tr > 200 years ΔQ > 50 m^3/s
Tsunami Inundation	Tsunami Inundation ΔH (m) Return Period of tsunami Tr (years)	Tr < 100 years ΔH < 1 m	Tr < 500 years 1 < ΔH < 2 m	Tr < 5000 years 2 < ΔH < 3 m	5000 < Tr < 10000 years 3 < ΔH < 4 m	Tr > 10000 years ΔH > 4 m

a_7 = River Flooding

a_8 = Tsunami Inundation

the impacts of coastal storms, which are exacerbated by the presence of the Boğaçay River.

Risk and Vulnerability Assessment Recent studies and observations have highlighted the accelerated coastal erosion at Konyaaltı Beach, with significant retreats of up to 50 m over the past 60 years, notably intensified by human activities such as the construction of nearby ports and the Boğaçay recreation area project. The erosion has been so severe that in some areas, the beach width has been reduced to the point where laying down a towel has become impossible. This erosion not only threatens the beach's tourism value but also poses risks to the urban infrastructure behind it. Flooding, particularly from the Boğaçay River, presents another significant risk. Heavy rainfall events have transformed streets into rivers, inundating urban areas and causing substantial damage. The construction of a sand storage dam in the Boğaçay bed has been proposed to mitigate the environmental effects of abandoned marina construction at the mouth and coast of Boğaçay, highlighting the need for integrated solutions to manage flooding risks. In response to these pressing challenges, this study emerges as a significant contribution to the field of coastal management. It proposes a hybrid model that addresses the multifaceted vulnerabilities facing Konyaaltı Beach. By integrating various disciplines and approaches, this model aims to provide a comprehensive and sustainable solution for coastal protection.

Hybrid Model for Coastal Management In seeking to overcome these challenges, this study introduces a novel hybrid model for vulnerability and risk assessment. The model comprises the following submodules:

1. **Predicting Coastal Storms**: Leveraging historical data and climate models to forecast the frequency, intensity,

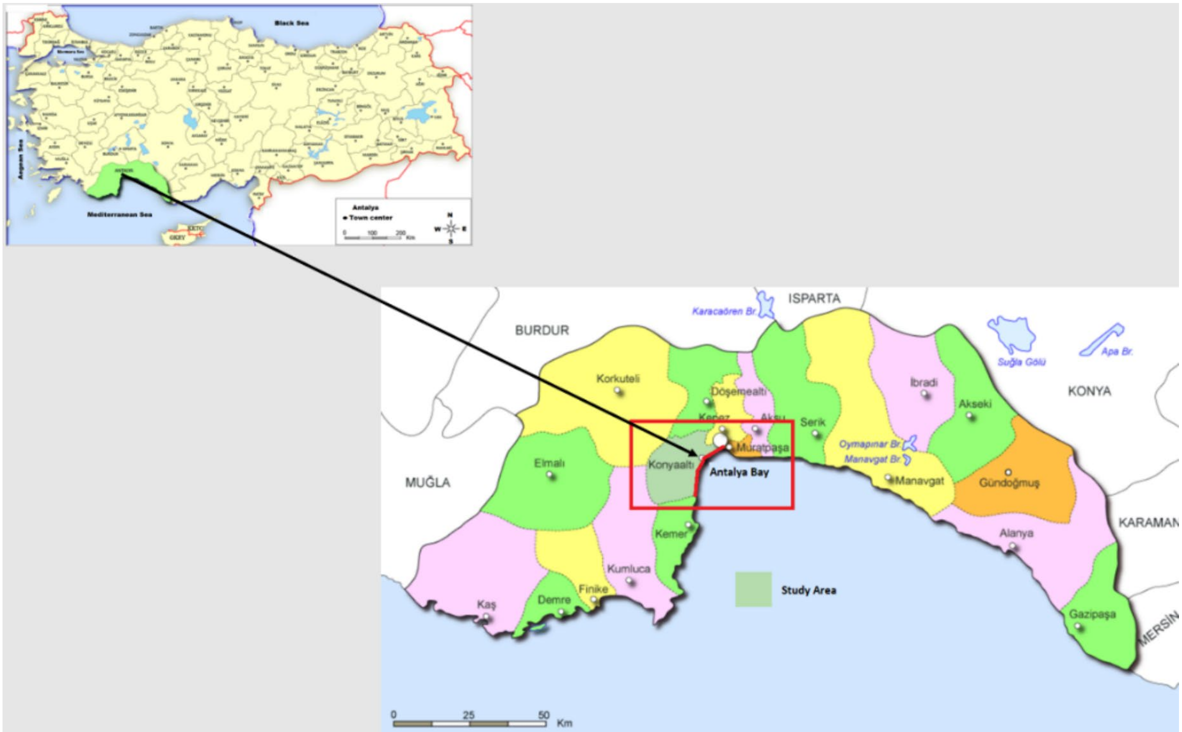

Fig. 5 Konyaaltı Beach of Antalya Bay located in the Mediterranean Sea

and impact of coastal storms on the Konyaaltı Beach area.

2. **Quantifying Sediment Transport Rate**: Assessing the movement of sediments along the coast to understand the dynamics of erosion and accretion, which are crucial for managing beach morphology and preventing erosion.
3. **Assessing Tsunami Inundation Severity**: Although less frequent, the potential impact of tsunamis on coastal areas necessitates the development of models to predict inundation areas and impact severity.
4. **Categorizing Storms Based on Beach Types**: Different beach types respond differently to storm events. Categorizing storms based on their impact on various beach types can aid in developing targeted management strategies.
5. **Enhancing Coastal Resilience**: Implementing strategies to increase coastal resilience by restoring sediment balance, allocating space for coastal processes, and internalizing coastal erosion costs in planning and investment decisions.

This comprehensive approach aims to address the multifaceted risks faced by the Konyaaltı Beach area, promoting sustainable coastal management practices that can safeguard the region's ecological, economic, and social values.

Application of ANFIS storm prediction module

Within the scope of this study, the wave data was obtained from the station named 'Antalya Bay Float Buoy' located in Antalya-Belek offshore 36°44′19.5"N 31°00′25.9"E geographical location. For the data set, 24-h daily data for the 2015 March-2017 January time interval were obtained from the measurements of the 'Antalya Bay Buoy' station. The largest wave height measured in the study area is 4.09 m, and the smallest wave height is 0.04 m with a standard deviation of 0.40 m. For 12-month wave data, in total 8779 significant wave heights for the years 2015–2016 were obtained. 6618 of them were used for the training phase of the ANFIS model and 2161 of them for the testing phase. The ANFIS models were developed by changing the membership function type and differentiating the time delays. RMSE, MAE, R, and R^2 statistical performance parameters were calculated for the models created and the results obtained are shown with the model types in Table 13. The scatter diagrams of models that gave the most successful results for train and testing among the examined models are given in Fig. 6. The advantages of artificial intelligence techniques are assessed through a comparison between real data and artificial intelligence-based prediction models. The Adaptive Neuro-Fuzzy Inference System (ANFIS) method was employed to obtain wave height estimations using various lag intervals.

The application of Gauss and Gumbel membership functions and hybrid optimization models were found to significantly improve the estimation results compared to other models. The results of the statistical comparison between the wave height estimations obtained using ANFIS and real data revealed that generally, determination coefficients of model results are surpassing 85%. ANFIS models can be considered suitable for forecasting the significant wave height parameter. The implementation of hybrid optimization models incorporating Gauss and Gumbel membership functions was found to perform superiorly in comparison to other model types. This research highlights the potential of ANFIS in addressing the difficulties associated with predicting wave heights, particularly in the face of climate change. These techniques can be refined by fine-tuning to further improve their accuracy and consistency for the Mediterranean Sea coasts of Turkey (Durap 2023).

Application of hydrodynamic coastal morphology module

Hourly wind data of ECMWF (European Centre for Medium-Range Weather Forecast) at every 0.1-degree horizontal grid spacing at the coordinate of 36.8°N-30.7°E for 30 years and fetch lengths were used to model wave heights, wave durations, and wave directions. Effective fetch distances (the distance over water that the wind blows in a single direction) in the studied coastal area are illustrated in Fig. 7 and presented in Table 14.

Effective Fetch Analysis: The effective fetch distances for Konyaaltı Beach, as depicted in Fig. 5, illustrate the extent of open water over which wind can blow to generate waves. The fetch distances are crucial for understanding the wave energy reaching the coast, which impacts coastal morphology and potential erosion. The longest fetch is observed in the SSE direction at approximately 655,797.6 m, indicating a significant potential for wave generation from this direction. Conversely, the shortest fetch is towards the west at 2,927.67 m, suggesting a limited wave influence from this direction. The variation in fetch distances across different directions (Table 14) is indicative of the anisotropic nature of wave exposure at Konyaaltı Beach, which can lead to varying degrees of coastal vulnerability along different segments of the beach.

The cosine average method has been applied to determine the effective fetch lengths in all directions for Konyaaltı Beach. Wave climate studies have been carried out by modeling data of 36.8°N-30.7°E coordinate by using Hydrotam-3D Model. Yearly and seasonal wave roses for Konyaaltı Beach are illustrated in Fig. 8. Based on the directional extreme value wave statistics, significant wave heights and mean wave periods according to 50-year and 100-year return periods are given in Fig. 9.

The annual and seasonal wave rose diagrams (Fig. 8) provide a comprehensive overview of wave climate, including wave height and directionality throughout the year. The annual wave rose indicates a predominant calm condition with a significant percentage of calm waves (Hs < 0.5 m), which suggests a generally low-energy wave environment. Seasonal variations are evident, with the winter season showing a higher occurrence of waves from the NNE direction and the summer season exhibiting a more diverse distribution of wave directions. These seasonal patterns are essential for predicting temporal changes in coastal morphology and identifying periods of increased vulnerability due to wave action.

Extreme Value Analysis Figure 7 presents the extreme value wave statistics for Konyaaltı Beach using the Gumbel distribution. The plot shows the relationship between significant wave height and return periods, providing a probabilistic assessment of wave heights expected over different time intervals. The high coefficient of determination ($R^2 = 0.95157$) indicates a good fit of the Gumbel distribution to the observed wave data. The analysis suggests that significant wave heights exceeding 5 m have a return period of approximately 50 years, which is critical information for long-term coastal management and planning. The extreme value analysis aids in understanding the risk of rare but high-impact wave events that can cause significant coastal change or damage.

From the wave transformation module, the potential wave power of the unit wave crest approaching Konyaaltı Beach is tabulated in Table 15. Directional Log-linear distribution equations of significant wave heights (Hs) and exceedance probabilities predictions obtained from modeling data are tabulated in Table 16.

In the context of assessing coastal vulnerability, the results presented in Table 16 indicate the potential wave power of unit wave crest approaching Konyaaltı Beach, measured in kilowatts per meter (kW/m). The table provides a detailed matrix of wave power across various wave heights (m) and wave periods (s). The wave heights range from 0.15 m to 4.15 m, and the wave periods span from 1 to 10 s.The data reveals that the highest wave power is associated with a wave height of 0.45 m and a wave period of 2 s, yielding a value of 284.5 kW/m. Conversely, the lowest non-zero values are observed at higher wave heights and longer wave periods, such as a wave height of 4.15 m and a wave period of 10 s, with a wave power of 6.9 kW/m.This information is critical for understanding the energy dynamics of waves impacting the coastline and can be used to predict the potential for erosion and other

Table 13 *ANFIS m*odels and their statistical performances in Hs prediction as compared with the real measurements at the testing stage

					TRAIN				TEST			
Model	MF	# of MF	Opt. Meth		RMSE	MAE	R	R2	RMSE	MAE	R	R2
Hs 4 2	gmbellmf	3 3	hybrid	constant	0.10712	0.06457	0.96675	0.9346	0.10149	0.06224	0.95677	0.9154
Hs 4 2	gaussmf	3 3	hybrid	constant	0.10719	0.06466	0.96675	0.9346	0.10172	0.06243	0.95656	0.915
Hs 4 2	trapmf	3 3	hybrid	constant	0.10799	0.06539	0.96623	0.9336	0.10272	0.06361	0.95567	0.9133
Hs 4 2	trimmf	3 3	hybrid	constant	0.10775	0.06464	0.96639	0.9338	0.1018	0.06228	0.9565	0.9149
Hs 4 2	gauss2mf	3 3	hybrid	constant	0.10704	0.06461	0.9668	0.9347	0.10163	0.06235	0.95666	0.9152
Hs 5 3	gmbellmf	3 3	hybrid	constant	0.13958	0.08561	0.94287	0.889	0.13005	0.08297	0.92806	0.8613
Hs 5 3	gaussmf	3 3	hybrid	constant	0.13971	0.08587	0.94276	0.8888	0.13023	0.0832	0.92785	0.8609
Hs 5 3	trapmf	3 3	hybrid	constant	0.13898	0.08553	0.9434	0.89	0.13077	0.08331	0.92731	0.5899
Hs 5 3	trimmf	3 3	hybrid	constant	0.13996	0.08574	0.94255	0.8884	0.13374	0.084	0.92369	0.8532
Hs 5 3	gauss2mf	3 3	hybrid	constant	0.13898	0.08549	0.9434	0.89	0.13028	0.08315	0.92785	0.8609
Hs 3 1	gmbellmf	3 3	hybrid	constant	0.06804	0.04054	0.98671	0.9736	0.07127	0.04029	0.97898	0.9584
Hs 3 1	gaussmf	3 3	hybrid	constant	0.06856	0.04056	0.98651	0.9732	0.07029	0.04008	0.97959	0.9596
Hs 3 1	trapmf	3 3	hybrid	constant	0.06779	00.04044	0.98681	0.9738	0.0714	0.04038	0.97893	0.9583
Hs 3 1	trimmf	3 3	hybrid	constant	0.0685	0.04047	0.98656	0.9733	0.07208	0.04039	0.97852	0.9575
Hs 3 1	gauss2mf	3 3	hybrid	constant	0.06833	0.04063	0.98661	0.9734	0.07124	0.0403	0.97903	0.9585
Hs 4 2	gmbellmf	2 2	hybrid	constant	0.10771	0.06483	0.96639	0.9339	0.1015	0.06234	0.95677	0.9154
Hs 4 2	gaussmf	2 2	hybrid	constant	0.10781	0.06474	0.96633	0.9338	0.1017	0.06234	0.95656	0.915
Hs 4 2	trapmf	2 2	hybrid	constant	0.10942	0.06615	0.9653	0.9318	0.10267	0.06413	09.95572	0.9134
Hs 4 2	trimmf	2 2	hybrid	constant	0.1081	0.06461	0.96613	0.9334	0.10195	0.06237	0.95635	0.9146
Hs 4 2	gauss2mf	2 2	hybrid	constant	0.10765	0.06489	0.96644	0.934	0.1015	0.0624	0.95677	0.9154
Hs 5 3	gmbellmf	3 3	backp	constant	0.1495	0.09171	0.93434	0.873	0.13444	0.08809	0.92336	0.8526
Hs 5 3	gaussmf	3 3	backp	constant	0.15129	0.09341	0.93274	0.87	0.13581	0.08948	0.92179	0.8497
Hs 5 3	trapmf	3 3	backp	constant	0.15723	0.08858	0.92763	0.8605	0.13167	0.08336	0.92634	0.8581
Hs 5 3	trimmf	3 3	backp	constant	0.07522	0.04384	0.98392	0.9681	0.07139	0.04217	0.97898	0.9584
Hs 5 3	gauss2mf	3 3	backp	constant	0.10298	0.04867	0.96974	0.9404	0.07566	0.04493	0.97647	0.9535
Hs 3 1	gmbellmf	3 3	hybrid	linear	0.06572	0.03986	0.98762	0.9754	0.07097	0.04032	0.97918	0.9588
Hs 3 1	gaussmf	3 3	hybrid	linear	0.06602	0.03999	0.98752	0.9752	0.07097	0.04039	0.97918	0.9588
Hs 3 1	gmbellmf	3 3	backp	linear	0.06999	0.04286	0.986	0.9722	0.07127	0.04217	0.97903	0.9585
Hs 3 1	gaussmf	3 3	backp	linear	0.06962	0.04264	0.98615	0.9725	0.07111	0.04212	0.97913	0.9587
Hs 3 1	gauss2mf	3 3	backp	linear	0.07002	0.04286	0.986	0.9722	0.07113	0.04213	0.97918	0.9588
Hs 3 1	gmbellmf	3 3	backp	linear	0.06999	0.04286	0.986	0.9722	0.07127	0.04217	0.97903	0.9585
Hs 3 1	gauss2mf	3 3	backp	linear	0.06963	0.04264	0.98615	0.9725	0.07101	0.04212	0.97913	0.9587
Hs 4 2	gmbellmf	3 3	hybrid	linear	0.10537	0.0638	0.96788	0.9368	0.101085	0.06242	0.95645	0.9148
Hs 4 2	gaussmf	3 3	hybrid	linear	0.10551	0.06376	0.96778	0.9366	0.10083	0.06223	0.95734	0.9165
Hs 4 2	trapmf	3 3	hybrid	linear	0.10568	0.0639	0.96768	0.9364	0.10108	0.06239	0.9573	0.9161
Hs 4 2	trimmf	3 3	hybrid	linear	0.10705	0.06446	0.9668	0.9347	0.10162	0.0623	0.95666	0.9152
Hs 4 2	gauss2mf	3 3	hybrid	linear	0.10559	0.06383	0.96773	0.9365	0.10105	0.06236	0.95713	0.9161
Hs 5 3 1	gmbellmf	3 3	hybrid	constant	0.06626	0.04015	0.98742	0.975	0.07243	0.0403	0.97831	0.9571
Hs 5 3 1	gaussmf	3 3	hybrid	constant	0.06697	0.04019	0.98717	0.9745	0.06821	0.03989	0.98077	0.9619
Hs 5 3 1	gauss2mf	3 3	hybrid	constant	0.06665	0.04047	0.98727	0.9747	0.07596	0.04058	0.97617	0.9529
Hs 4 3 1	gmbellmf	3 3	hybrid	constant	0.06697	0.04045	0.98717	0.9745	0.07174	0.04026	0.97872	0.9579
Hs 4 3 1	gaussmf	3 3	hybrid	constant	0.0674	0.04023	0.98697	0.9741	0.07003	0.04004	0.97974	0.9599
Hs 4 3 1	gauss2mf	3 3	hybrid	constant	0.06637	0.0401	0.98737	0.9749	0.07086	0.04011	0.97923	0.9589

forms of coastal damage. The variation in wave power with respect to wave height and period is indicative of the complex interplay between these factors and their collective impact on coastal vulnerability. The results from this table were integrated into coastal vulnerability models to enhance the accuracy of predictions regarding shoreline changes and to inform the development of risk mitigation strategies for coastal regions.

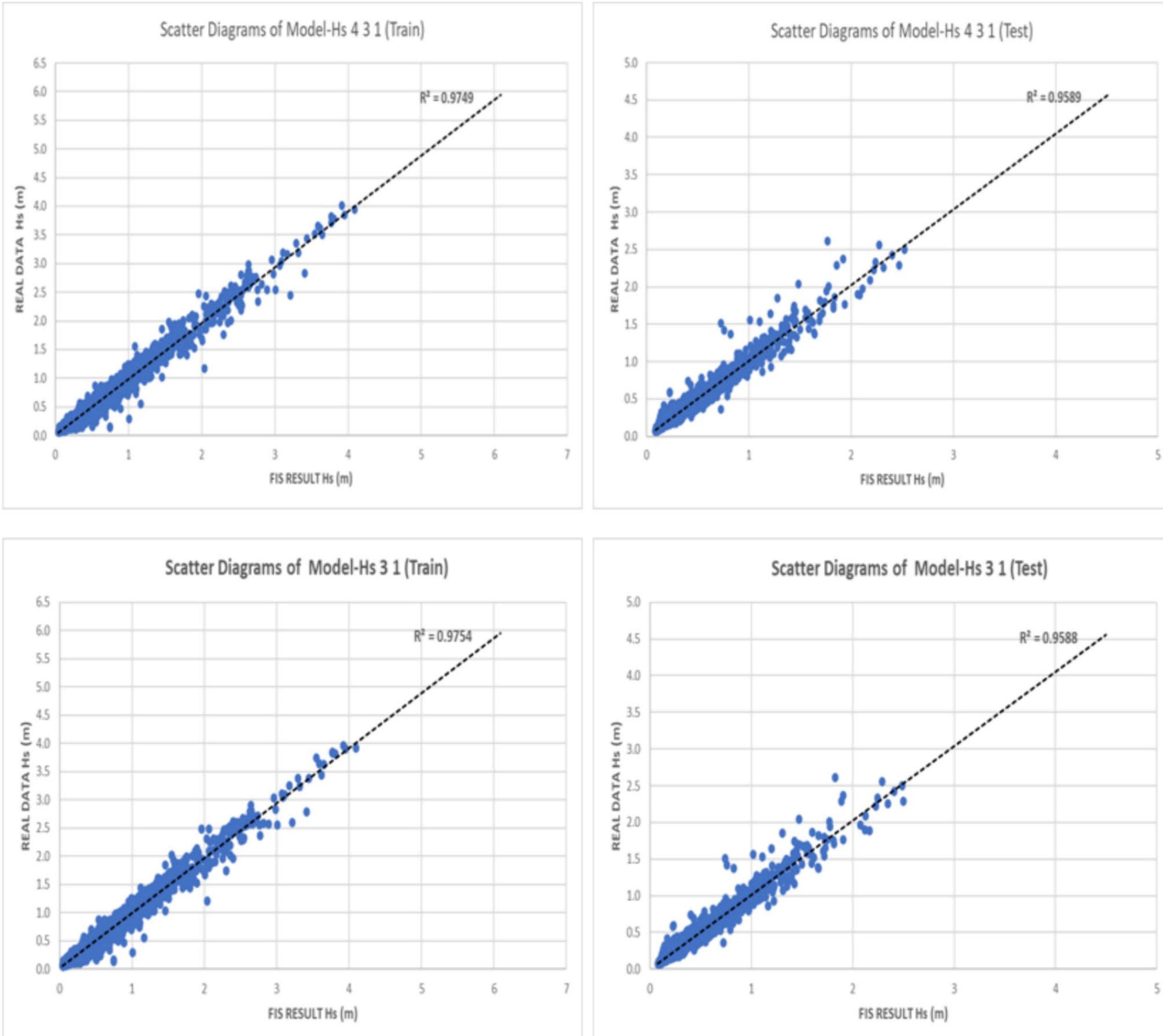

Fig. 6 Comparison of ANFIS Models (Hs-3–1 and Hs-4–3-1) results having Gumbel and Gauss membership functions with the real measurements at the testing stage

The results from Fig. 11 can be used in conjunction with Fig. 10 to enhance the assessment of coastal vulnerability in the following ways:

Directional Wave Data: Table 16 provides predictions of significant wave heights and periods from various directions, which is essential for understanding the directional impact of waves on the coastline. This information can help identify the most vulnerable sections of the coast based on the predominant wave approach directions.

Exceedance Probabilities: The exceedance probabilities offer insight into the likelihood of certain wave conditions occurring within specific time frames. This probabilistic approach is crucial for risk assessment and long-term coastal planning.

Model Validation and Prediction: The equations in Table 16 were used to validate the wave power predictions in Table 15. By comparing the predicted significant wave heights and periods with the measured wave power, researchers can assess the accuracy of their models.

Integrated Risk Assessment: By combining the wave power data from Table 15 with the exceedance probabilities and significant wave heights from Table 16, a comprehensive risk assessment were conducted. This integrated approach allows for the evaluation of both the

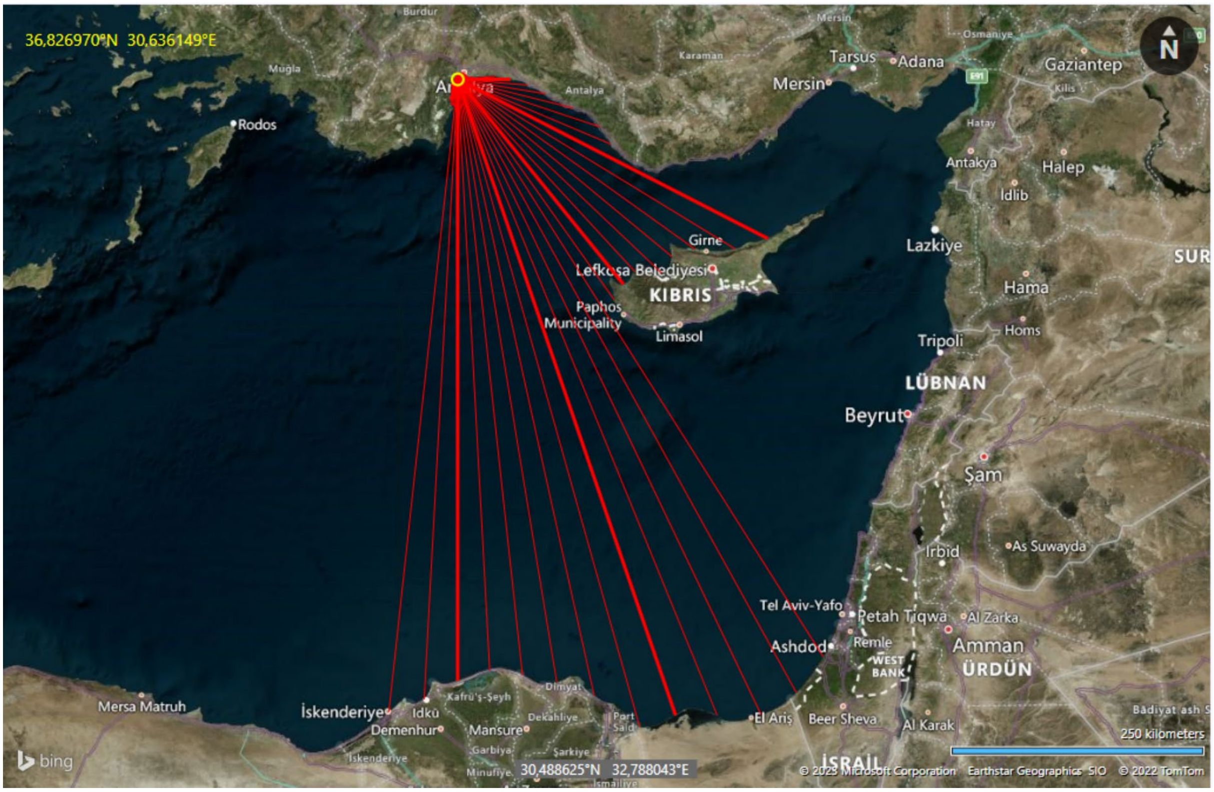

Fig. 7 Effective Fetch distances of Konyaaltı Beach

Table 14 Effective fetch distances of Konyaaltı Beach (m)

Direction	Angle (°)	Fetch (m)
E	90	53,532.61
ESE	112.5	229,819.9
SE	135	377,951.3
SSE	157.5	655,797.6
S	180	517,741.1
SSW	202.5	19,921.74
SW	225	9664.65
WSW	247.5	5532.68
W	270	2927.67

immediate and long-term risks associated with coastal vulnerability.

Coastal Management Strategies: By identifying areas at higher risk of erosion or inundation on a site-specific basis, the combined data from both tables were informed coastal management strategies. This can guide the implementation of protective measures, such as seawalls or dune reinforcement, and influence zoning regulations for coastal development (Table 17).

Table 16 presents a detailed quantitative analysis of sediment transport rates surrounding Konyaaltı Beach. It delineates the volume of sediment transported annually in cubic meters from various directional sectors, specifically highlighting transport from SW to ENE and vice versa. The data reveals a net transport rate of 450,444.88 m3/year and a gross transport rate of 635,557.73 m3/year. This bidirectional sediment transport information plays a pivotal role in comprehending the sediment budget and morphological alterations along the coastline. Consequently, these findings were incorporated into the assessment of coastal vulnerability along 11 profiles of Konyaaltı Beach.

Application of tsunami inundation module

The application of the tsunami inundation module has been extended to evaluate the coastal vulnerability of Konyaaltı Beach, a popular recreational area within Antalya Bay. The model, powered by an Artificial Neural Network (ANN-2), predicts the potential inundation heights resulting from tsunamis triggered by earthquakes of varying intensities, ranging from 1 to 6. These predictions are crucial for understanding the trends in coastal vulnerability and for implementing effective disaster risk reduction strategies. The results, which are detailed in Table 18, provide

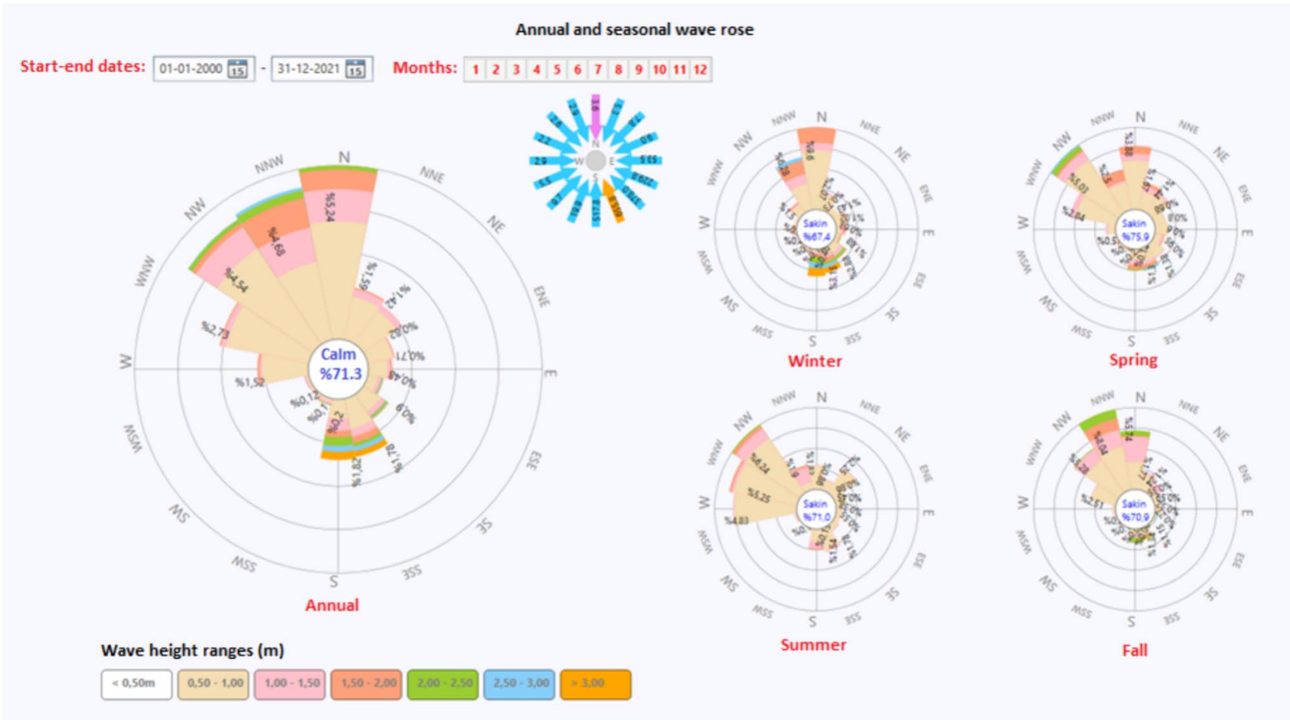

Fig. 8 Yearly and seasonal wave roses (Calm Hs < 0.5 m) for Konyaaltı Beach

Fig. 9 Extreme value wave statistics of all wave directions (Gumbel Distribution)

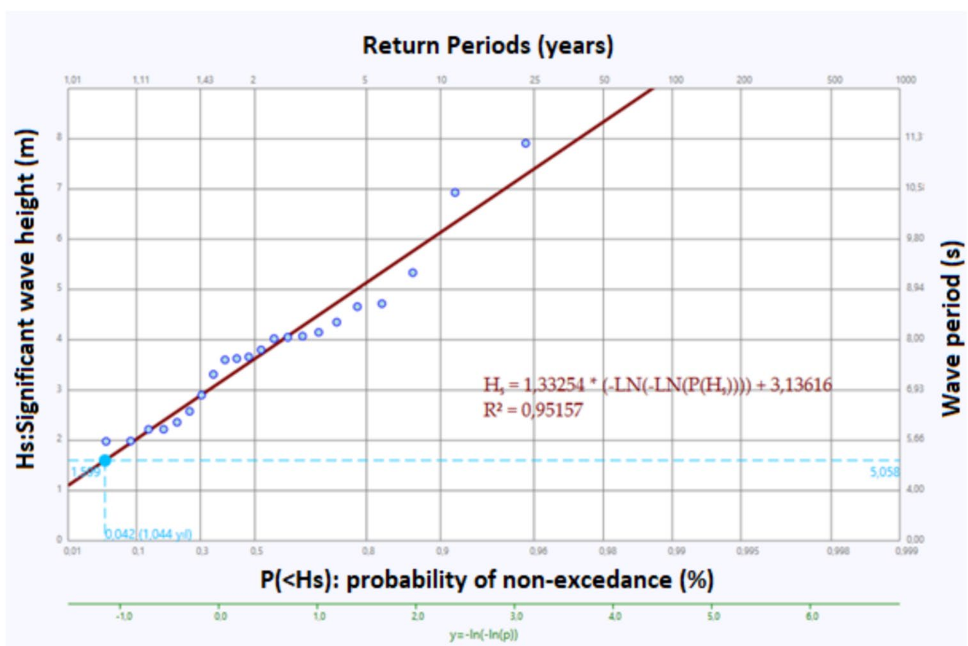

insights into the resilience of Konyaaltı Beach's infrastructure and natural defenses, and they underscore the need for ongoing monitoring and adaptive management to protect this valuable coastal zone.

Application of BN-coastal vulnerability module

In four different profiles of Konyaaltı beach, profiles are evaluated to determine whether they are reflective or dissipative beaches. The results are compared by hazard assessments that were obtained by using a Coastal Vulnerability

Table 15 Potential Wave Power of unit wave crest approaching Konyaaltı Beach (kW/m)

Wave Height (m) / Wave Period (s)	1	2	3	4	5	6	7	8	9	10
0.15	2997	0	0	0	0	0	0	0	0	0
0.35	388	304.8	32.3	0	0	0	0	0	0	0
0.45	231.8	284.5	44.1	0	0	0	0	0	0	0
0.55	152.1	256	34.3	0	0	0	0	0	0	0
0.65	59.6	345.4	10	0	0	0	0	0	0	0
0.75	0	76.5	142.4	10.6	0	0	0	0	0	0
0.85	0	39.8	429	56.1	0	0	0	0	0	0
0.95	0	18.6	364	57.3	0	0	0	0	0	0
1.05	0	10.3	29.9	359.4	0	0	0	0	0	0
1.15	0	4.5	13.6	339.2	0	0	0	0	0	0
1.25	0	0.8	9.3	230.7	0	0	0	0	0	0
1.35	0	0.2	2.2	197.3	0	0	0	0	0	0
1.45	0	0.1	0	236	0	0	0	0	0	0
1.55	0	0.1	0	38.4	233.1	0	0	0	0	0
1.65	0	0	0	15.2	165.8	0	0	0	0	0
1.75	0	0	0	56.1	2.5	39.5	0	0	0	0
1.85	0	0	0	0	2.6	31	0	0	0	0
1.95	0	0	0	0	1.6	193	0	0	0	0
2.05	0	0	0	0	1.7	37.2	0	0	0	0
2.25	0	0	0	0	1.8	1	20	0	0	0
2.35	0	0	0	0	0	0	56.4	0	0	0
2.45	0	0	0	0	0	0.3	4.8	33.6	0	0
2.55	0	0	0	0	0	0.2	18.6	29.1	0	0
2.65	0	0	0	0	0	0.1	0	32	0	0
2.75	0	0	0	0	0	0.2	0	14.6	0	0
2.85	0	0	0	0	0	0.1	0	14.8	0	0
2.95	0	0	0	0	0	0.1	0	6.3	0	0
3.05	0	0	0	0	0	0	0	13.7	0	0
3.15	0	0	0	0	0	0	0	5.5	0	0
3.25	0	0	0	0	0	0	0	1.1	12	0
3.35	0	0	0	0	0	0	0	0	5.8	0
3.45	0	0	0	0	0	0	0	0	10	0
3.55	0	0	0	0	0	0	0	0	17.4	0
3.65	0	0	0	0	0	0	0	0	8.8	0
3.75	0	0	0	0	0	0	0	0	15.2	0
3.85	0	0	0	0	0	0	0	0	17.7	0
3.95	0	0	0	0	0	0	0	0	1.3	9.7
4.05	0	0	0	0	0	0	0	0	0.3	4.9
4.15	0	0	0	0	0	0	0	0	0.2	6.9

Assessment Model (CVAM) as illustrated in Fig. 10. In this figure the prior displays the probability of the dataset without any constraints and the posterior displays the likelihood that is dependent on the erosion indices for Levels 4 and 5.

The New BN-based Coastal Risk Assessment Framework Network was applied to the hazard assessment of Konyaaltı Beach by using the flow chart given in Fig. 10. The results of the BN network are presented in Fig. 11, where the application of the developed classification system for the beach profiles based on storm effects is presented for Konyaaltı beach. The potential coastal erosion profiles for four prominent Konyaaltı beaches were determined and illustrated in Fig. 12. Researchers used a 1:25,000 scale topographic map dated 1934 and a 2022 Digital Globe satellite image to compare the changes in the profiles. Upon juxtaposing these two different measurements, the edge of

Table 16 Directional Log-linear distribution equations of significant wave heights (Hs) and exceedance probabilities of predictions obtained from modeling ECMWF Data

Dir	Cumulative Log-Linear Equation		1 h/year		5 h/year		10 h/year	
			H_s (±m) %90 Confidence	T_m (s)	H_s (±m) %90 Confidence	T_m (s)	H_s (±m) %90 Confidence	T_m (s)
E	H_s = -0.994	-0.322Ln(P(H_s))	1.930 ± 0.112	5.164	1.130 ± 0.048	3.888	0.660 ± 0.049	2.916
ESE	H_s = -2.872	-0.658Ln(P(H_s))	3.100 ± 0.251	6.513	1.460 ± 0.105	4.396	0.500 ± 0.150	2.497
SE	H_s = -3.047	-0.750Ln(P(H_s))	3.760 ± 0.196	6.970	1.900 ± 0.091	4.844	0.800 ± 0.112	3.053
SSE	H_s = -4.467	-1.197Ln(P(H_s))	6.400 ± 0.182	9.727	3.420 ± 0.078	6.912	1.670 ± 0.066	4.662
S	H_s = -4.930	-1.363Ln(P(H_s))	7.450 ± 0.191	10.152	4.060 ± 0.083	7.370	2.060 ± 0.061	5.147
SSW	H_s = -2.470	-0.517Ln(P(H_s))	2.230 ± 0.239	5.599	0.940 ± 0.093	3.307	0.180 ± 0.160	1.206
SW	H_s = -1.579	-0.333Ln(P(H_s))	1.440 ± 0.174	4.439	0.620 ± 0.098	2.661	0.130 ± 0.169	1.030
WSW	H_s = -2.550	-0.496Ln(P(H_s))	1.950 ± 0.328	5.318	0.720 ± 0.182	3.028	0.610 ± 0.161	2.180
W	H_s = -0.777	-0.317Ln(P(H_s))	2.100 ± 0.173	5.604	1.310 ± 0.083	4.296	0.850 ± 0.066	3.353

the coast was drawn, and cross-sections were measured at 11 points along the coast.

Results

The changes have been evaluated, and by using the new BN-based methodology constructed, the projections of shoreline changes have been obtained. These changes offered an insight into future shoreline changes as given for various periods in Fig. 13. In Fig. 13, future scenarios have been established by considering four future periods (5, 20, 50, and 100 years). Each profile has different shoreline changes (m) predicted in its prediction period. For example, the shoreline changes in profile 3 within 50 years are estimated as 15m. It is predicted that shoreline changes will drastically increase when the period reaches 50 years. Each cross-section (1 to 11) is conforming to its wave condition. Dredging operations or groin construction can accelerate these shoreline changes.

The intensity of the shoreline disturbance is expected to grow with an increasing likelihood of erosion as illustrated in Fig. 14. Points 4, 5, 6, and 11 all contribute to hazards that the shore faces. As a result of the increased likelihood of erosion at these four locations, they are found as reflective shoreline points. The rest of the points are considered a dissipative beach.

In addition, if groins will be constructed at the outlet of the Boğaçay River for flood control as illustrated in Fig. 15, disaster indices will significantly increase. The current pattern of the bottom layer at the steady state due to 10 m/s wind speed from North northwest (NNW) direction in Section "Introduction" is demonstrated in Fig. 15a, and the shoreline changes due to Boğaçay groins are shown in Fig. 15b. At the end of the fifth year, the change in the coastline, which is expected to be seen within 20 years, occurs within 5 years. Accordingly, the probability of occurrence of the 5th category disaster index exceeds 45%. This comparison can be achieved because of combining three-dimensional hydrodynamic current and sediment transport models of shoreline changes with the Bayesian networks.

The major floods occur due to extreme storms which affect both Konyaaltı Beach and simultaneously create extreme floods in the main branch of Boğaçay River, which has a width of 200 m and enters the sea from Section "Introduction" with a length of 750 m at the beach. In addition, the Boğaçay basin accumulates an enormous amount of sediment that affects the beach section. According to the General Directorate of State Hydraulic, the amount of sediment accumulated in 6 years between 2009 and 2016 is 450000 m^3. According to this data, an average of 64.280 m^3 of sediment accumulates in the main branch of Boğaçay each year.

The shoreline change is measured at eleven distinct cross-sections along the coast, providing a detailed spatial analysis of the coastal evolution. The projections are made for five different time periods: 5, 20, 50, and 100 years into the future. Figure 13 involves a combination of historical data analysis, coastal dynamics modeling, and consideration of factors such as sea-level rise, sediment supply, and human interventions.

The results are as follows:

- At the 5-year mark, the shoreline change is minimal across all cross-sections, with the most significant change being approximately 2.4 m at cross-section 4.
- For the 20-year projection, the changes become more pronounced, especially at cross-sections 4 and 7, with changes around 11 m and 9.4 m, respectively.
- The 50-year projection shows a general increase in shoreline change, with cross-section 4 experiencing the most substantial change at approximately 36 m.
- The 100-year projection indicates the most significant changes, with cross-section 4 again showing the largest change at around 76 m. Notably, cross-sections 1, 2,

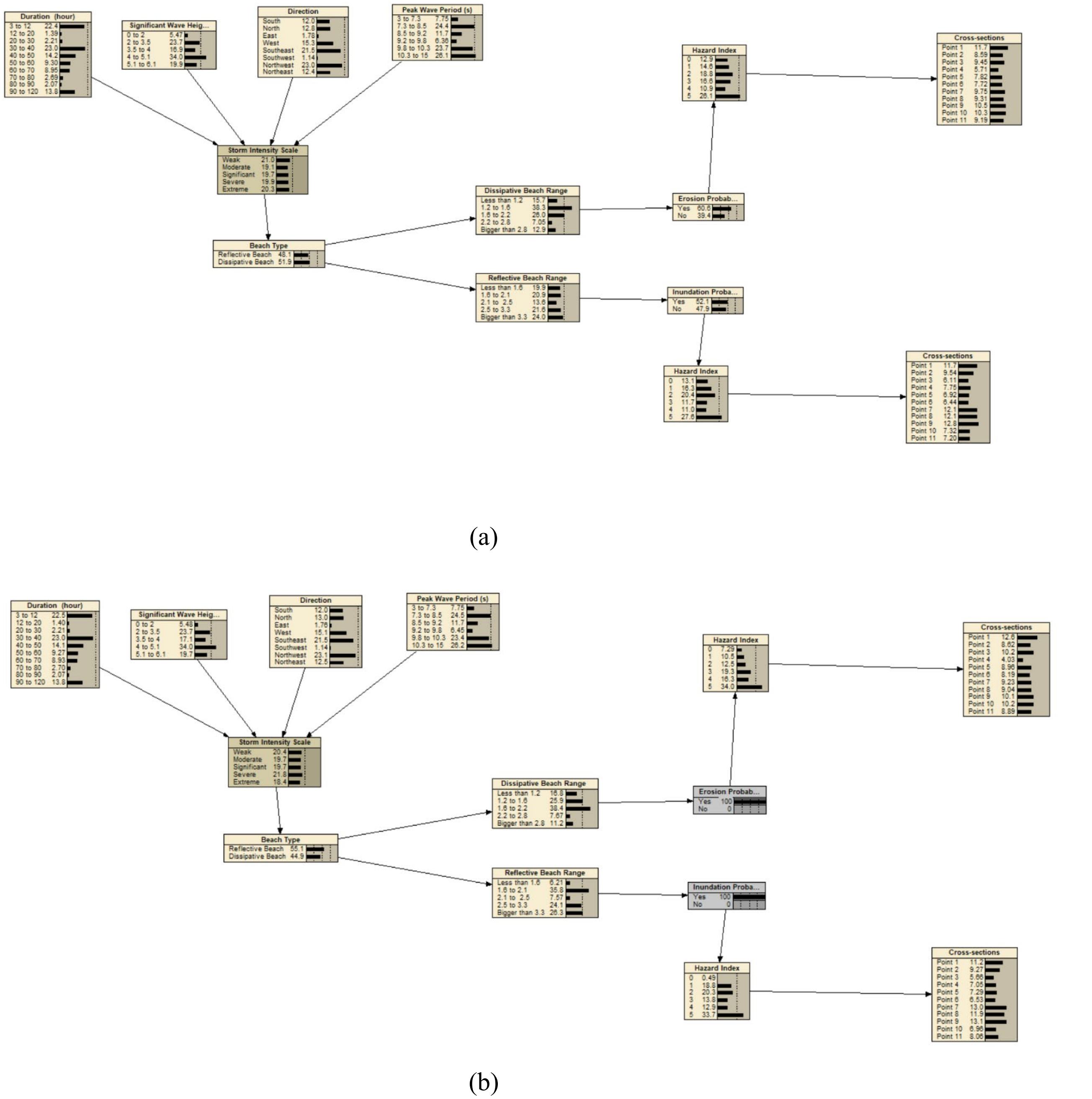

Fig. 10 The BN-based Coastal Risk Assessment Framework Network applied to hazard assessment of Konyaaltı Beach **a**) Unconstrained network (prior) **b**) Constrained network for the worst-case scenario (posterior)

and 11 also exhibit considerable changes, ranging from 43 to 66 m.

It suggests that certain areas of the Konyaaltı coast are more susceptible to change over time, particularly cross-section 4, which consistently shows the highest projected changes. This is highly likely due to various factors such as the geomorphology of the area, the presence of coastal structures, presence of river, and natural processes like longshore drift.The relatively stable projections at the 5-year mark across all cross-sections suggest that short-term changes are not as significant. However, as the time horizon extends to 20, 50, and 100 years, the cumulative effects of coastal processes and possibly climate change become more apparent.

Table 17 The average annual sediment transport rates (m^3/s) of Konyaaltı Beach

Direction	Transport from SW to ENE	Transport from ENE to SW
ENE	-	7913.59
E	-	8935.27
ESE	-	68142.94
SE	-	7564.62
SSE	220956.02	-
S	281753.16	-
SSW	40098.45	-
SW	193.67	-
Total	543001.3	92556.43
Net	450444.88	
Gross	635557.73	

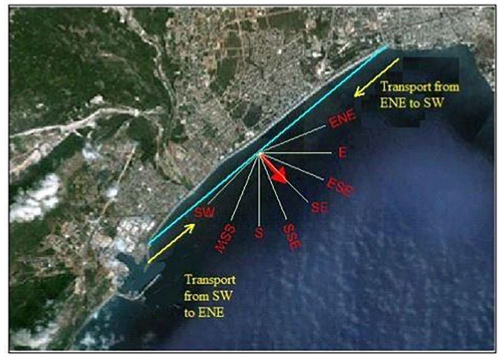

Table 18 Tsunami/Seiche risk of the Seferihisar Bay obtained from the ANN Module

Tsunami Intensity (i)	Tsunami Height (m)	Occurrence probability
1	0.5213	0.0057
2	2.4765	0.0036
3	5.9555	0.00145
4	8.6757	0.00115

Based on the analysis of the Fig. 14, the following conclusions were drawn:

Spatial Heterogeneity: The risk of hazards along the shoreline is spatially heterogeneous, with some areas being more susceptible to higher hazard indexes than others such as river areas

Risk Management Implications: It suggests that risk management strategies should be tailored to specific cross-sections of the shoreline, with more resources allocated to areas that exhibit a higher probability of severe hazards.

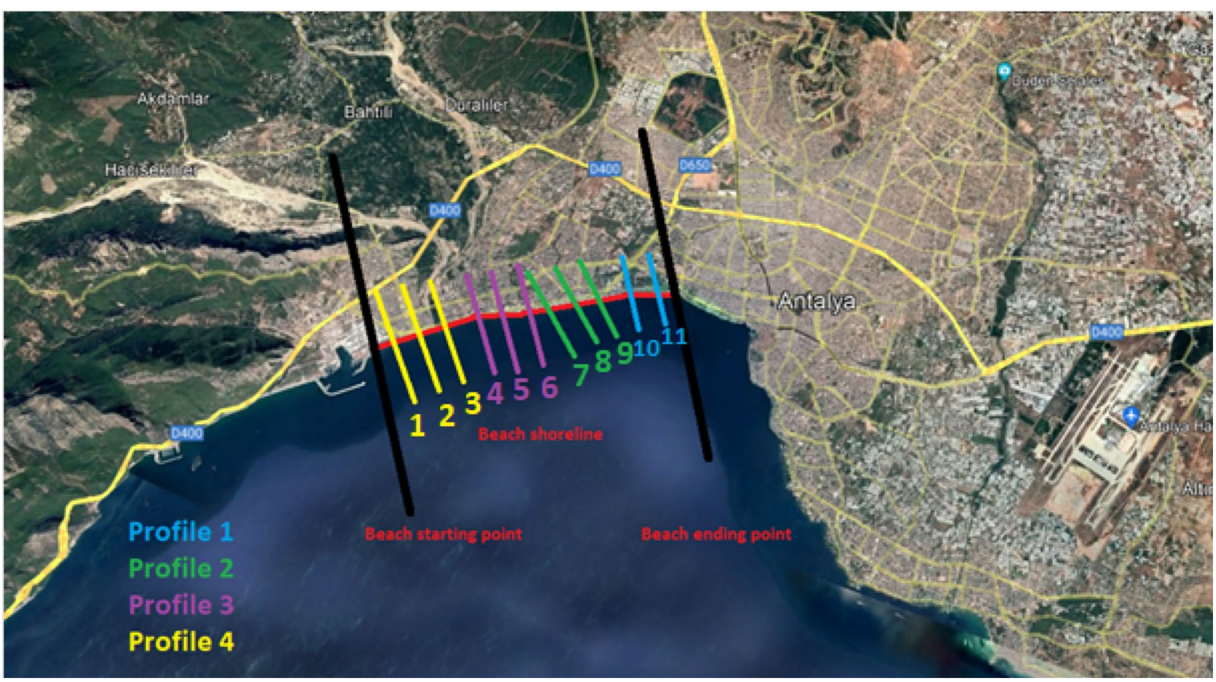

Fig. 11 The application of the developed classification system for the beach profiles based on storm effects

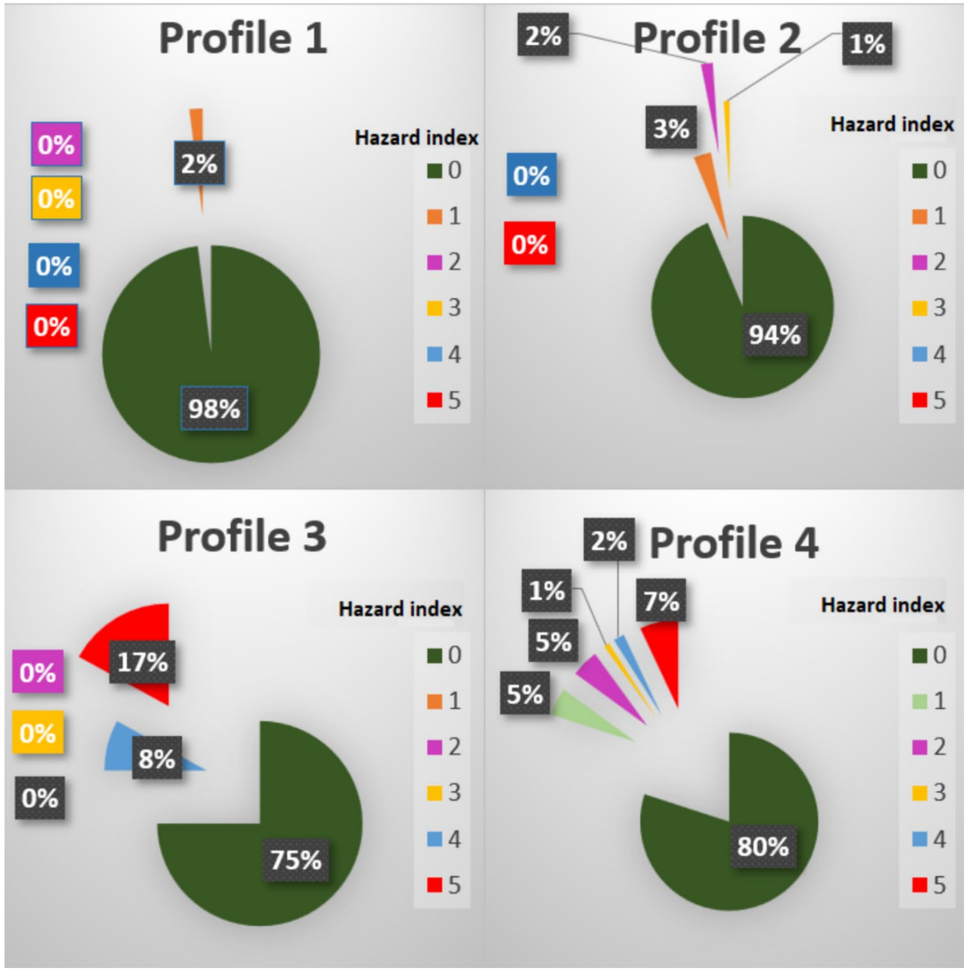

Fig. 12 The potential coastal erosion profiles for four prominent Konyaaltı beaches

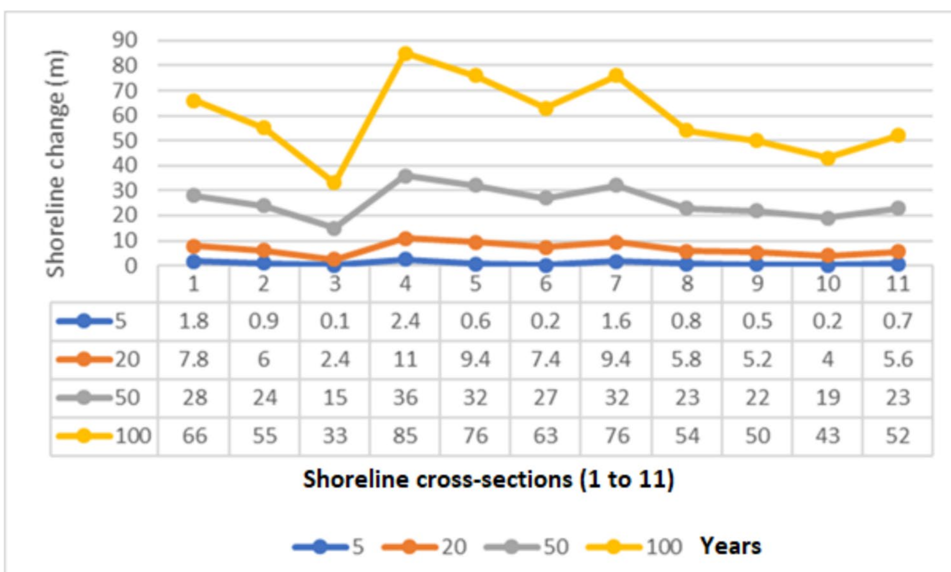

Fig. 13 Five future periods (years) that show how the beaches will change at Konyaaltı coast

The historical context provided mentions major floods due to extreme storms, with significant discharges affecting Konyaaltı Beach and the Boğaçay River. The events of 25 December 2003, as well as more recent floods in December 2018 and February 2019, underscore the importance of

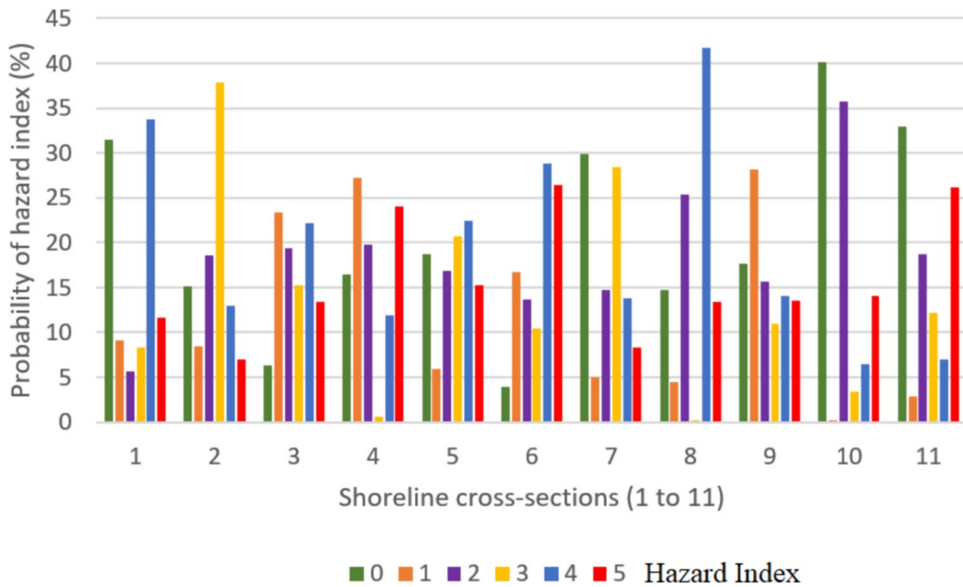

Fig. 14 Hazard indexes of 0 to 5 for each cross-section of the shoreline

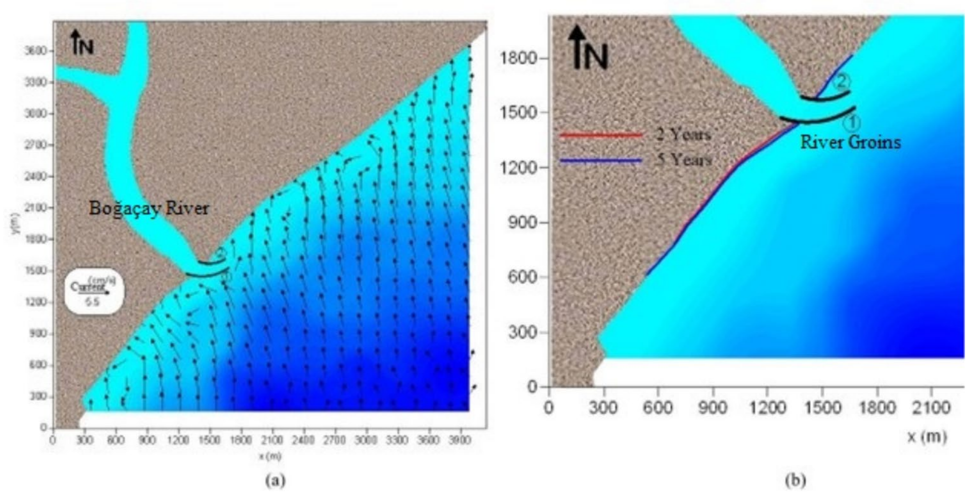

Fig. 15 Assessment of coastal vulnerability: impact of river groins on sediment dynamics and shoreline evolution near the boğaçay river. **a** Current pattern of the bottom layer at the steady state due to 10 m/s wind speed from North northwest (NNW) direction in Section "Introduction" (**b**) Shoreline changes expected with the construction of Boğaçay groins

understanding and predicting the impacts of both natural and anthropogenic factors on coastal vulnerability (Photo 1).

According to the criteria of Table 19, each variable was allocated a score of 1–5. Assuming that the flow rate and return period are 100 m^3 and 100 years respectively. The vulnerability concerning river floods will be 2 (a7 = 2). Similarly, in case that tsunami inundation height is $2 < \Delta H < 3$ m and period Tr < 5000, falling into class 3, thus a8 = 3.

The heatmap provides a detailed visual representation of the coastal vulnerability at different points (P1 to P12) based on various parameters and the Coastal Vulnerability Index (CVI). The parameters considered include geomorphology, sea-level change, shoreline displacement, tidal range, one-year maximum wave height, river flooding, tsunami inundation, and beach slope. Each parameter is rated on a scale from 1 (very low) to 5 (very high), and the overall CVI is calculated for each point (Fig. 16).

Following that, the Coastal Vulnerability Index (CVI, a metric, is used to assess the relative vulnerability of coastal areas to a combination of factors, including geomorphology, sea-level change, shoreline displacement, tidal range, wave height, river flooding, tsunami inundation, and beach slope.

This analysis ranked twelve coastal profiles based on their CVI scores. Profile 3 and profile 4 were found to be the most vulnerable (CVI = 45, Rank 1), followed by profiles 5 (CVI = 22.0, Rank 2) and 2 (CVI = 21, Rank 3). Profiles 8, 9, and 10 exhibited the least vulnerability (CVI = 10, Rank 7) (Fig. 17).

It has been determined that point 3 and are more likely to be at risk of being vulnerable due to the presence of the Boğacay river. So, while calculating the coastal vulnerability index, it is of the utmost significance to take into consideration both the impact of river flooding and the height of tsunami inundation. Figure 18 displays the coastal vulnerability

Photo 1 Extreme flood occurred in Boğaçay River on 7 February 2019 at Section "Introduction" of Konyaaltı Beach

Table 19 Boğaçay River expected flow rates, water level (Y), and velocity (for 260 m width)

R_p(years)	2	5	10	25	50	100	500
Q(m^3/sn)	660	970	1162	1399	1571	1736	2133
Y(m)	1.74	2.19	2.44	2.73	2.92	3.1	3.51
V(m/sn)	1.46	1.70	1.83	1.97	2.07	2.15	2.34
Risk (%)	99.9905	98.17	86.5	55.1	33	18.1	3.9

index over a time horizon of 10 years, taking into consideration the expected implications that climate change and global warming will have on the values of each component. Ten years scenario is given in the following figure:

The projected CVI scores for a ten-year scenario show significant changes, implying that the current management practices or natural resilience may not be maintaining the vulnerability at a steady state. Points with higher values in parameters such as river-attached area, sea level change, and shoreline displacement may require more focused attention to mitigate potential impacts. Furthermore, given the introduction of two novel variables into the vulnerability and risk assessment methodology, a sensitivity analysis was conducted to isolate their specific contributions to the overall CVI scores (Fig. 19).

Key observations:

River Flooding (a_7): A positive correlation is evident between the CVI and the a_7 parameter. As the value of a_7 increases from 1 to 5, a commensurate rise in the CVI is observed. This signifies a high degree of sensitivity within the CVI framework to alterations in riverine flooding. Consequently, higher a_7 values correspond to elevated vulnerability indices.

Tsunami Inundation (a_8): Similar to the a_7 parameter, the CVI demonstrates a positive correlation with the a_8 parameter. An increment in the value of a_8 from 1 to 5 is mirrored by a corresponding increase in the CVI. This observation suggests that the CVI exhibits comparable sensitivity to changes in tsunami inundation. In essence, higher a_8 values translate to heightened vulnerability indices.

Discussions

The development and application of the Hybrid Model and Bayesian Network Model have provided significant insights into coastal vulnerability, particularly in terms of storm effects, flooding, and erosion. Based on the findings and methodologies employed in this study, several tailored management strategies can be proposed to enhance coastal resilience and sustainability.

1. Adaptive Infrastructure Design

   Given the predictive capabilities of the model regarding significant wave heights and storm classifications, coastal infrastructure should be designed with adaptability in mind. This includes the construction of seawalls, breakwaters, and dune reinforcements that can be adjusted or enhanced based on updated risk assessments. The model's ability to predict wave parameters and storm impacts allows for a proactive approach in infrastructure planning and design, ensuring that coastal defenses can withstand future conditions predicted by the model.
2. Zoning and Land Use Regulations

   The study's findings on coastal vulnerability and sediment transport rates should inform zoning and land use regulations in coastal areas. Areas identified as highly

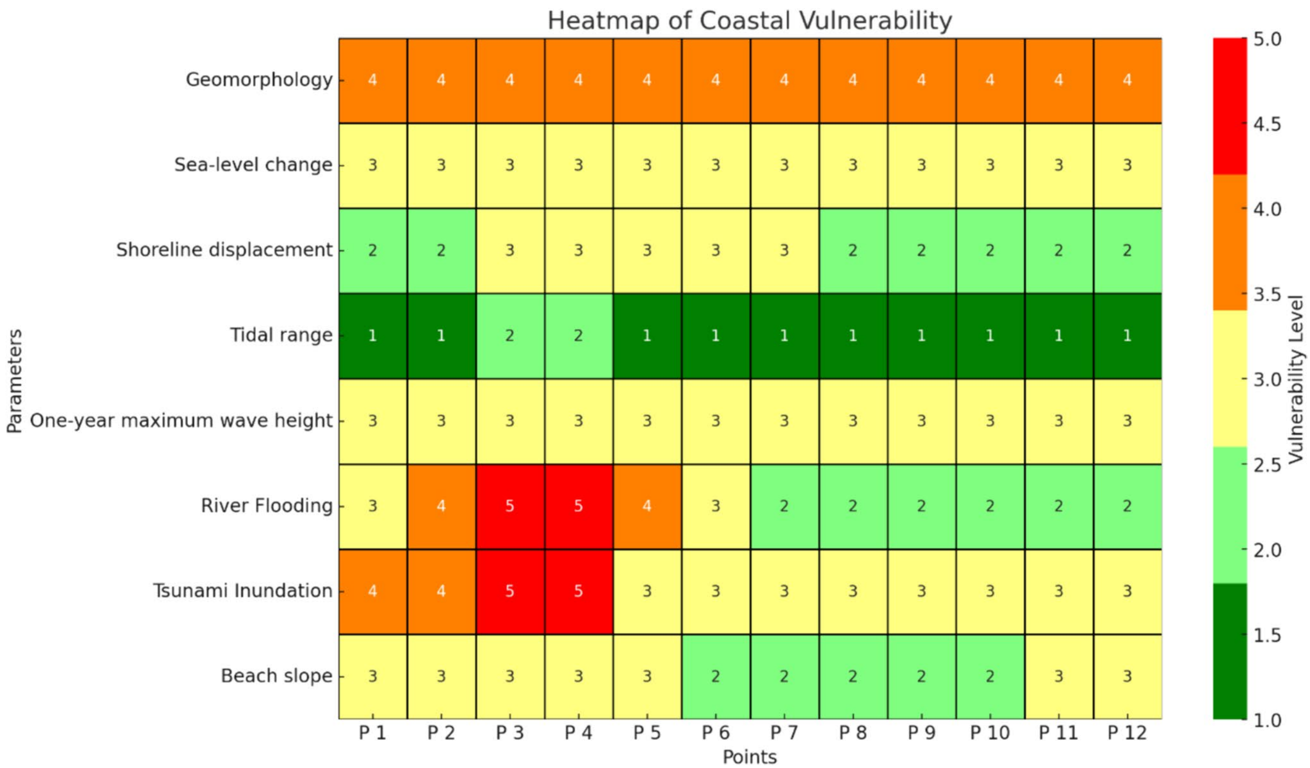

Fig. 16 Vulnerability level assessment along the Konyaaltı Beach, showing variation in vulnerability of each parameters

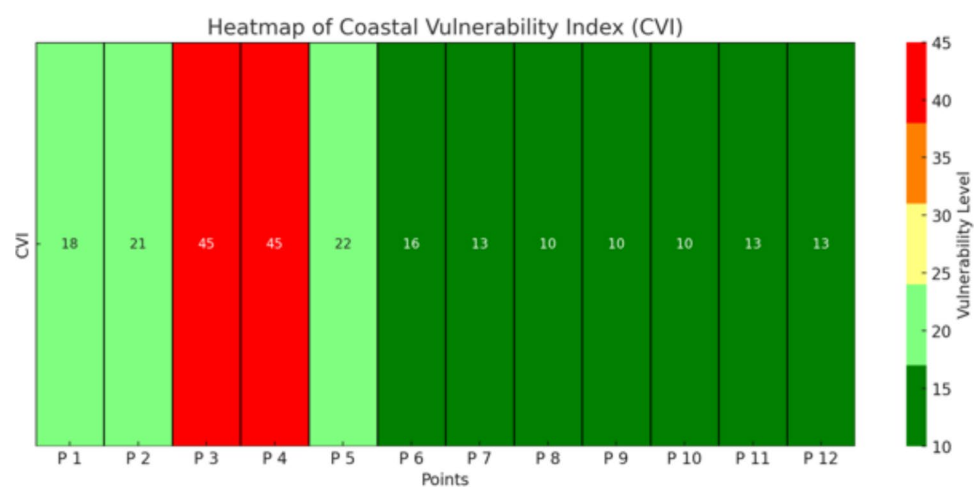

Fig. 17 Heatmap of Coastal Vulnerability Index (CVI) for profiles of Konyaaltı Beach

vulnerable to erosion or inundation should be subject to stricter development controls, while promoting the conservation of natural buffers such as mangroves and dunes. Implementing setback zones based on the model's

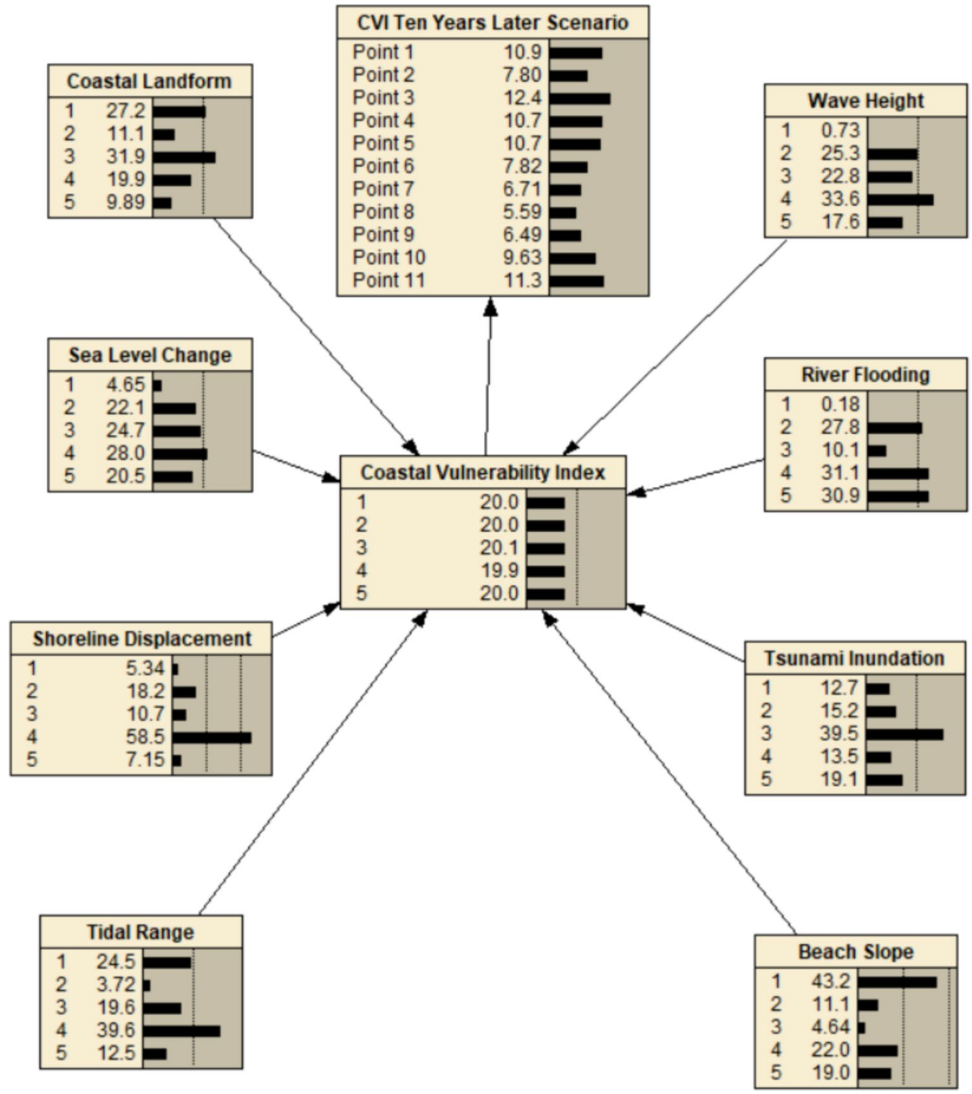

Fig. 18 Future scenario of CVI Index for 11 points on Konyaaltı Beach

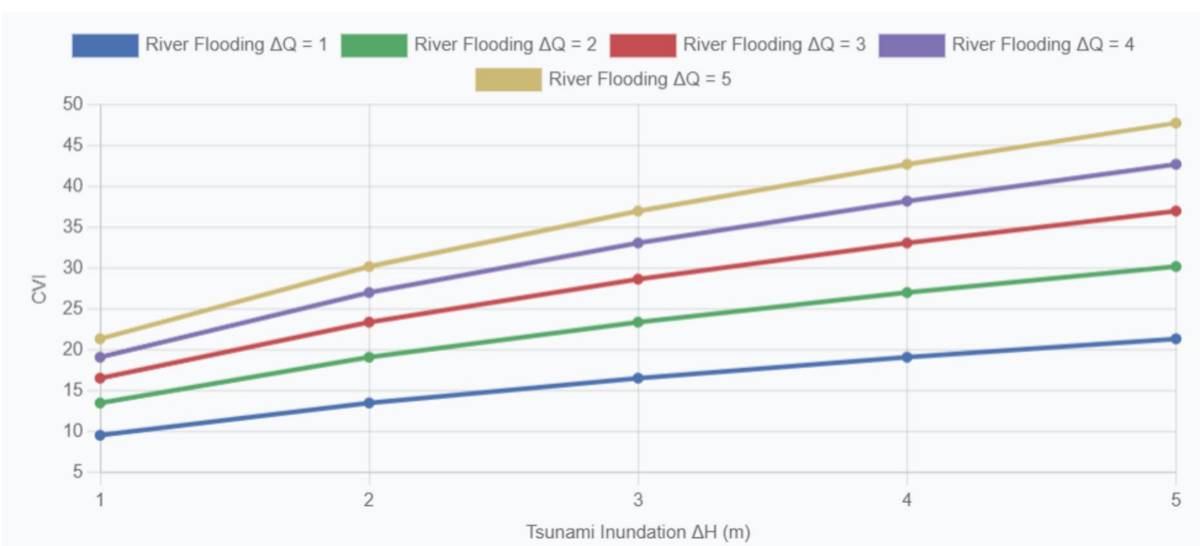

Fig. 19 CVI vs tsunami inundation for different river flooding discharge rate (sensitivity analysis)

risk assessments can reduce the exposure of properties and infrastructure to coastal hazards.

3. Integrated Risk Management

   The integrated approach to risk assessment demonstrated by combining wave power data, exceedance probabilities, and significant wave heights offers a comprehensive framework for coastal risk management. This strategy involves the continuous monitoring of coastal conditions, the application of the model for updated risk assessments, and the implementation of risk mitigation measures such as emergency preparedness plans and community awareness programs. By understanding both immediate and long-term risks, coastal communities can better prepare for and respond to coastal hazards.

4. Ecosystem-based Management

   The study highlights the importance of considering the natural dynamics of coastal systems in management strategies. Ecosystem-based management approaches, such as the restoration of coastal habitats and the implementation of nature-based solutions (e.g., living shorelines), can enhance coastal resilience. These strategies not only provide protection against erosion and flooding but also support biodiversity and offer recreational and economic benefits to coastal communities.

5. Collaborative Governance and Stakeholder Engagement

   Effective management strategies require the involvement of multiple stakeholders (Ekmekcioğlu 2024), including government agencies, local communities, scientists, and the private sector. The model's findings should be communicated to all stakeholders to foster a collaborative approach to coastal management. Engaging stakeholders in the decision-making process ensures that management strategies are well-informed, socially acceptable, and economically viable.

6. Continuous Monitoring and Model Refinement

   The dynamic nature of coastal systems necessitates ongoing monitoring and model refinement. As new data becomes available and as coastal conditions change, the model should be updated to reflect these changes. Continuous monitoring of coastal parameters and the incorporation of feedback from management interventions will enhance the model's accuracy and relevance, ensuring that management strategies remain effective over time.

Conclusions

This paper discusses the development of a HM and BNM to assess coastal vulnerability, integrating environmental parameters like wind, wave, current, and sediment transport. The study focuses on risk assessment for storm effects, flooding, and erosion, evaluating coastal response to storm impact and developing a multipurpose model for Coastal Vulnerability Index (CVI) assessment. Key points from the paper include:

Storm Definition and Analysis: Storms are defined as wave events with specific characteristics, and the study analyzes storm impacts using cluster analysis and supervised categorization to understand storm energy contents.

Wave Prediction Models: The paper highlights the importance of predicting Significant Wave Heights (Hs) for coastal engineering design, discussing the challenges of direct measurement and the use of numerical wave prediction models incorporating various parameters.

ANFIS Models for Wave Prediction: The study utilizes Adaptive Network-Based Fuzzy Inference System (ANFIS) models for wave height estimation, emphasizing their effectiveness in predicting missing wave data along the Mediterranean coast.

Coastal Vulnerability Assessment: Bayesian Networks are employed to assess coastal vulnerability, considering uncertainties related to prediction models, climatic conditions, and coastline morphology. The BN-based approach enables a more accurate characterization of system response and risk assessment at a regional scale.

The integration of hydrodynamic modeling, Bayesian networks, and ANFIS within the Hybrid Model provides a robust framework for assessing coastal vulnerability and informing sustainable coastal management practices. The findings underscore the need for ongoing monitoring, model refinement, and collaborative governance to enhance coastal resilience against dynamic environmental forces.

The research aims to provide guidance for coastal communities in mitigating hazards' impact on urban developments by offering comprehensive risk assessments and management strategies based on detailed analyses of environmental parameters and storm characteristics.

Funding Open access funding provided by the Scientific and Technological Research Council of Türkiye (TÜBİTAK).

Data availability The data used in this study were obtained from Turkish Meteorological Portal and ECMWF. The specific datasets employed in our analysis can be located through their titles or by searching relevant keywords on the portal.

Declarations

Competing interests The author declare that it has no known competing financial interests or personal relationships that could have appeared to influence the work reported in this paper.

References

Arda T, Bayrak OC, Uzar M (2024) Analyzing coastal vulnerability using analytic hierarchy process and best-worst method: a case study of the Marmara Gulf region. Arab J Sci Eng. https://doi.org/10.1007/s13369-024-09128-w

Aykut F, Tezcan D (2024) Evaluating sea level rise impacts on the Southeastern Türkiye coastline: a coastal vulnerability perspective. PFG – J Photogramm Remote Sens Geoinformation Sci. https://doi.org/10.1007/s41064-024-00284-0

Balas L (2004) Modelling of interaction between surface waves and mud layer. 618–621. https://doi.org/10.1007/978-3-540-24687-9_86

Balas L, Özhan E (2003) A baroclinic three dimensional numerical model applied to coastal lagoons. 205–212. https://doi.org/10.1007/3-540-44862-4_23

Balas CE, Ergin A (2003) Rubble Mound Breakwaters Under Tsunami Attack. Submarine Landslides and Tsunamis. Springer, Netherlands, Dordrecht, pp 293–302. https://doi.org/10.1007/978-94-010-0205-9_31

Balas L, Özhan E (2001) Applications of a 3-D numerical model to circulation in coastal waters. Coast Eng J 43:99–120. https://doi.org/10.1142/S0578563401000293

Balas L, Özhan E (2002) Three-dimensional modelling of stratified coastal waters. Estuar Coast Shelf Sci 54:75–87. https://doi.org/10.1006/ecss.2001.0832

Briones-Peñalver A-J, Prokopchuk L, Samoilyk I (2023) Strategic vectors of coastal tourism development as a blue economy component in the international dimension. J Environ Manag Tour 14:2473. https://doi.org/10.14505/jemt.v14.6(70).01

Chen H, Li D, Chen Y, Zhao Z (2023) Spatial-Temporal Evolution Monitoring and Ecological Risk Assessment of Coastal Wetlands on Hainan Island, China. Remote Sens (Basel) 15:1035. https://doi.org/10.3390/rs15041035

Durap A (2023) A comparative analysis of machine learning algorithms for predicting wave runup. Anthropocene Coasts 6:17. https://doi.org/10.1007/s44218-023-00033-7

Durap A, Balas CE (2022) Risk assessment of submarine pipelines: A case study in Turkey. Ocean Eng 261:112079. https://doi.org/10.1016/j.oceaneng.2022.112079

Durap A, Balas CE, Çokgör Ş, Balas EA (2023) An integrated Bayesian risk model for coastal flow slides using 3-D hydrodynamic transport and Monte Carlo simulation. J Mar Sci Eng 11:943. https://doi.org/10.3390/jmse11050943

Ekmekcioğlu Ö (2024) Discovering the perception differences of stakeholders on the sustainable and innovative stormwater management practices. Water Resour Manage 38:2527–2544. https://doi.org/10.1007/s11269-024-03783-2

Filippaki E, Tsakalos E, Kazantzaki M, Bassiakos Y (2023) Forecasting impacts on vulnerable shorelines: vulnerability assessment along the coastal zone of Messolonghi area—Western Greece. Climate 11:24. https://doi.org/10.3390/cli11010024

Gornitz V (1991) Global coastal hazards from future sea level rise. Palaeogeogr Palaeoclimatol Palaeoecol 89:379–398. https://doi.org/10.1016/0031-0182(91)90173-O

Hanak E, Moreno G (2012) California coastal management with a changing climate. Clim Change 111:45–73. https://doi.org/10.1007/s10584-011-0295-2

Koroglu A, Ranasinghe R, Jiménez JA, Dastgheib A (2019) Comparison of coastal vulnerability Index applications for Barcelona Province. Ocean Coast Manag 178:104799. https://doi.org/10.1016/j.ocecoaman.2019.05.001

Kosenius A-K, Markku O (2015) Ecosystem benefits from coastal habitats—A three-country choice experiment. Mar Policy 58:15–27. https://doi.org/10.1016/j.marpol.2015.03.032

Lapietra I, Rizzo A, Colacicco R, Dellino P, Capolongo D (2023) Evaluation of social vulnerability to flood hazard in Basilicata region (Southern Italy). Water (Basel) 15:1175. https://doi.org/10.3390/w15061175

Lin N, Emanuel K, Oppenheimer M, Vanmarcke E (2012) Physically based assessment of hurricane surge threat under climate change. Nat Clim Chang 2:462–467. https://doi.org/10.1038/nclimate1389

Mafi-Gholami D, Zenner EK, Jaafari A, Riyahi Bakhtyari HR, Tien Bui D (2019) Multi-hazards vulnerability assessment of southern coasts of Iran. J Environ Manage 252:109628. https://doi.org/10.1016/j.jenvman.2019.109628

Mani Murali R, Ankita M, Amrita S, Vethamony P (2013) Coastal vulnerability assessment of Puducherry coast, India, using the analytical hierarchical process. Nat Hazard 13:3291–3311. https://doi.org/10.5194/nhess-13-3291-2013

Mendoza ET, Jiménez JA (2009) Regional vulnerability analysis of Catalan beaches to storms. Proc Inst Civ Eng - Marit Eng 162:127–135. https://doi.org/10.1680/maen.2009.162.3.127

Mohanty UC, Bhaskaran PK, Mohapatra M, Sahu SC (2020) Guest editorial to the special issue of natural hazards: climate change and coastal vulnerability. Nat Hazards 102:553–555. https://doi.org/10.1007/s11069-020-04065-x

Özyurt G, Ergin A (2010) Improving coastal vulnerability assessments to sea-level rise: a new indicator-based methodology for decision makers. J Coast Res 262:265–273. https://doi.org/10.2112/08-1055.1

Paprotny D, Terefenko P, Giza A, Czapliński P, Vousdoukas MI (2021) Future losses of ecosystem services due to coastal erosion in Europe. Sci Total Environ 760:144310. https://doi.org/10.1016/j.scitotenv.2020.144310

Sheaves M, Baker R, Nagelkerken I, Connolly RM (2015) True value of estuarine and coastal nurseries for fish: incorporating complexity and dynamics. Estuaries Coasts 38:401–414. https://doi.org/10.1007/s12237-014-9846-x

Sheik Mujabar P, Chandrasekar N (2013) Coastal erosion hazard and vulnerability assessment for southern coastal Tamil Nadu of India by using remote sensing and GIS. Nat Hazards 69:1295–1314. https://doi.org/10.1007/s11069-011-9962-x

Sudha Rani NNV, Satyanarayana ANV, Bhaskaran PK (2015) Coastal vulnerability assessment studies over India: a review. Nat Hazards 77:405–428. https://doi.org/10.1007/s11069-015-1597-x

Tahri M, Maanan M, Maanan M, Bouksim H, Hakdaoui M (2017) Using Fuzzy Analytic Hierarchy Process multi-criteria and automatic computation to analyse coastal vulnerability. Prog Phys Geogr: Earth Environ 41:268–285. https://doi.org/10.1177/0309133317695158

Toimil A, Losada IJ, Camus P, Díaz-Simal P (2017) Managing coastal erosion under climate change at the regional scale. Coast Eng 128:106–122. https://doi.org/10.1016/j.coastaleng.2017.08.004

Torresan S, Critto A, Dalla Valle M, Harvey N, Marcomini A (2008) Assessing coastal vulnerability to climate change: comparing segmentation at global and regional scales. Sustain Sci 3:45–65. https://doi.org/10.1007/s11625-008-0045-1

Zhang K, Douglas BC, Leatherman SP (2004) Global warming and coastal erosion. Clim Change 64:41–58. https://doi.org/10.1023/B:CLIM.0000024690.32682.48